HOKKAIDO UNIVERSITY

Title	Petrology, trace element abundances and oxygen isotopic compositions of a compound CAI-chondrule object from Allende
Author(s)	Wakaki, S.; Itoh, S.; Tanaka, T.; Yurimoto, H.
Citation	Geochimica et Cosmochimica Acta, 102, 261-279 https://doi.org/10.1016/j.gca.2012.10.039
Issue Date	2013-02-01
Doc URL	http://hdl.handle.net/2115/51784
Type	article (author version)
File Information	GCA102_261-279.pdf

Instructions for use

Hokkaido University Collection of Scholarly and Academic Papers : HUSCAP

Petrology, trace element abundances and oxygen isotopic compositions of a compound CAI-chondrule object from Allende

S. Wakaki[*1], S. Itoh[1], T. Tanaka[2] and H. Yurimoto[1]

[1] Department of Natural History Sciences, Hokkaido University, Sapporo 060-0810, Japan

[2] Department of Earth and Environmental Sciences, Nagoya University, Chikusa, Nagoya 464-8602, Japan

* Corresponding author. Present address: Kochi Institute for Core Sample Research, Japan Agency of Marine-Earth Science and Technology (JAMSTEC), 200 Monobe Otsu, Nankoku 783-8502, Japan. Tel.: +81-88-878-2214. E-mail address: wakaki@jamstec.go.jp

ABSTRACT

We report the petrology, trace element abundances and oxygen isotopic characteristics of a compound CAI-chondrule object, WI-025, found in the Allende CV3 chondrite. WI-025 is an irregularly shaped inclusion consisting of three texturally and chemically distinct portions; the interior portion, the igneous rim and the intermediate zone between these two portions. The interior portion consists of anorthite, spinel, olivine and Al-bearing low-Ca pyroxene. Major element chemistry of the interior portion corresponds to that of Al-rich chondrules and is intermediate between fine-grained spinel-rich CAIs and ferromagnesian chondrules. The interior portion has abundant ^{16}O-rich spinel (Δ^{17}O = -14.2 to -24.7) and shows a group II CAI-like REE composition. These observations indicate that the interior portion contains a CAI component formed by fractional condensation. Major and trace element chemistry of the interior portion indicate that the CAI had subsequently assimilated chondrule materials through partial melting. The maximum heating temperature of the partial melting is estimated to be about 1400 ˚C, similar to the maximum heating temperature of Type-B CAIs. The oxygen isotopic compositions of the olivine and low-Ca pyroxene (Δ^{17}O = -6.3) in the interior portion indicate that the partial melting and chondrule assimilation took place

under moderately ^{16}O-poor nebular gas. The igneous rim is texturally and chemically similar to ferromagnesian chondrules and entirely surrounds the interior portion. The oxygen isotopic compositions of the olivine and low-Ca pyroxene in the igneous rim are indistinguishable from those of the interior olivine and Al-bearing low-Ca pyroxenes. These observations indicate that a chondrule material, which was melted in the same nebular gas as the interior portion, was accreted to the interior portion. The intermediate zone is a reaction zone accompanying the igneous rim formation. The formation history of WI-025 can be summarized as 1) original CAI formation, 2) partial melting and chondrule assimilation, 3) igneous rim formation and 4) secondary alteration on the parent body.

.

1. INTRODUCTION

Calcium-aluminum-rich inclusions (CAIs) and chondrules are considered to have formed in the solar nebula (e.g. Scott and Krot, 2005). Although both CAIs and chondrules record high-temperature processes, such as condensation, evaporation and melting that occurred in the solar nebula at the early stage of solar system's evolution,

1 they differ in their chemical and isotopic compositions as well as in their petrology.

2 CAIs are composed of refractory minerals, such as spinel, melilite and
3 Al-Ti-rich diopside, are enriched in refractory elements and generally show an ^{16}O-rich
4 oxygen isotopic composition ($\delta^{17, 18}$O ~ -50 ‰; Yurimoto et al., 2008). The fractionated
5 refractory trace element compositions of CAIs indicate that some CAIs (or the
6 precursors) were formed by condensation (Tanaka and Masuda, 1973; Boynton, 1975;
7 Davis and Grossman, 1979; Kornacki and Fegley; 1986). CAIs having igneous texture
8 were formed by complete or partial melting and subsequent crystallization. The melting
9 conditions of the igneous CAIs are estimated by crystallization experiments using
10 igneous CAI analogs. Such experiments suggest that Type-B CAIs, typical igneous
11 CAIs, have been heated to a maximum temperature of 1400 ˚C for no more than a few
12 tens of hours and subsequently cooled at 2 ~ 50 degrees per hour (Stolper and Paque,
13 1986; Jones et al, 2000; Connolly and Burnett, 2003).

14 Chondrules are ferromagnesian objects mainly composed of olivine and
15 low-Ca pyroxene, show an ^{16}O-poor bulk oxygen isotopic composition ($\delta^{17, 18}$O = +10 ~
16 -10 ‰; Yurimoto et al., 2008) and were formed by melt crystallization. The melting
17 conditions of ferromagnesian chondrules estimated from crystallization experiments

using chondrule analogs consist of a maximum heating temperature of 1500 ~ 1850 ˚C, a heating time of several seconds to a few minutes and a cooling rate of 500 ~ 1000 degrees per hour (Jones et al, 2000; Hewins et al., 2005; Connolly et al., 2006).

The timing of CAI and chondrule crystallization can be precisely determined by both Pb-Pb and Al-Mg chronometers. The Pb-Pb ages of CAIs are at 4567.2 - 4568.5 Ma (Amelin et al.; 2002; Bouvier et al., 2007; Jacobsen et al., 2008; Amelin et al.; 2010), whereas the Pb-Pb ages of chondrules are slightly younger ranging from 4564.7 Ma to 4566.6 Ma (Amelin et al.; 2002; Amelin and Krot, 2007; Connelly et al., 2008). Al-Mg systematics indicate that the crystallization ages of chondrules are 1 - 3 million years younger than the crystallization ages of CAIs (MacPherson et al., 1995; Kita et al., 2005; Jacobsen et al., 2008; Villeneuve et al., 2009). These observations show that CAIs and chondrules melted and crystallized under different conditions and at different times in the solar nebula. However, details of the astrophysical processes and heating mechanisms that caused the melting of CAIs and chondrules are not well understood, although there are several suggested models. Moreover, whether the astrophysical processes that led to the melting of the CAIs and chondrules are identical or not remains unclear (Jones et al., 2000; Connolly et al., 2006).

Aluminum-rich chondrules, which have a chemical composition intermediate between CAIs and ferromagnesian chondrules, represent another set of objects formed by melting and crystallization in the solar nebula. The mixing of CAI and chondrule materials has been proposed as one possible process explaining the origin of some portion of the Al-rich chondrules, based on their major element compositions (Sheng et al., 1991; Macpherson and Huss, 2005). The mixing of CAI and chondrule materials is also speculated to have played a role in the formation of type-C CAIs, which have a chemical composition similar to that of Al-rich chondrules (Krot et al., 2008). CAI material signatures are found in some ferromagnesian and Al-rich chondrules, with a Group-II-like fractionated REE composition reported in ferromagnesian chondrules from Allende and Felix (CO3) (Rubin and Wasson, 1987a; Misawa and Nakamura, 1988). Refractory precursor components of chondrules are inferred from trace element studies and factor analysis (Rubin and Wasson, 1987a). Evidence of the mixing of CAI and ferromagnesian chondrule materials can also be observed directly in CAI-chondrule compound objects. Such objects include CAIs containing relict chondrule fragments and chondrules containing relict CAI fragments or CAI traces (Sheng et al., 1991; Misawa and Fujita, 1994; Maruyama et al., 1999; Maruyama and Yurimoto, 2003; Itoh and

Yurimoto, 2003; Krot et al., 2005; Krot et el., 2006). These observations suggest that the mixing of CAIs and ferromagnesian chondrules, which have distinct origins, is a process occurred in the solar nebula. Since CAI-chondrule compound objects contain materials related to both CAIs and ferromagnesian chondrules, the formation history of such compound objects may provide a link between the formation processes of CAIs and those of chondrules and may also provide insights into the formation of Al-chondrules and Type-C CAIs.

Despite the importance of their formation process, the major element, trace element and O isotopic characteristics of CAI-chondrule compound objects have not been studied comprehensively. We report here petrological, bulk trace element and oxygen isotopic studies of a new CAI-chondrule compound object found in Allende (CV3). The object consists of an Al-rich chondrule-like interior portion and a surrounding igneous rim of ferromagnesian chondrule-like composition. Petrology and oxygen isotopic composition of the interior portion indicates that the interior portion is a partially melted CAI-chondrule mixture. The purpose of the study is to determine the formation history of this compound object.

2. EXPERIMENTAL

2. 1. Petrological observation and major element analysis

The inclusion named WI-025 was found on a pair of sliced Allende slabs. A polished thick section was prepared from one of the slabs and the other slab was kept for bulk INAA and subsequent analyses. Petrology of the inclusion was studied on the polished thick section using a JEOL JSM-7000F field-emission scanning electron microscope (FE-SEM) equipped with an Oxford INCA energy dispersive spectrometer (EDS). Major element microanalyses of minerals were performed with FE-SEM-EDS using a 15 kV accelerating voltage, 0.9 nA beam current and 120 sec counting time. Bulk major element compositions of the inclusion were estimated from multiple measurements covering the whole inclusion using a rastered and defocused beam. X-ray elemental maps were acquired by FE-SEM-EDS using a 10 nA beam current. X-ray elemental map of a region of interest was taken with a counting time of 0.5 sec/pixel. Modal composition was estimated from a combined Mg-Al-Ca x-ray elemental map of the whole inclusion by counting the pixels for a specific mineral.

2. 2. Trace element analysis

Bulk trace element abundances in the interior portion of the inclusion were measured by instrumental neutron activation analysis (INAA). A small portion (0.21 mg) of the interior part of the inclusion was scraped away with high-purity Ti tweezers under a binocular microscope. GSJ reference rock JB-1a and solution reagents of platinum group elements (including Re, Os and Ir), Au and rare earth elements (REE) were used as standards. The sample and standards were sealed in high-purity silica tubes. Solution standards were mixed and infiltrated into a small piece of filter paper and evaporated before sealing. The sample and standards were irradiated for 30 hours at the JRR-3 Reactor of Japan Atomic Energy Research Institute with a thermal neutron flux of 1×10^{14} neutrons/cm^2/sec. The irradiated sample and standards were measured three times using a Ge semiconducting detector with a SEIKO EG&G activation analysis system in Nagoya University: at about 5, 9 and 45 days after irradiation and with counting times of about 4, 14, 14 hours/sample, respectively. The blank contribution from the active silica tubes used for sealing was smaller than the analytical uncertainty in all measured elements and was thus negligible. Measured elements, measured nuclides, half-life and γ-ray energy are summarized in Table 1.

2. 3. Oxygen isotope analysis

Oxygen isotope analysis was performed in situ using the Hokkaido University Cameca ims 1270 ion microprobe. The primary ion beam was 200 pA mass filtered $^{133}Cs^+$ ions at an accelerating potential of 20 keV. Typical primary beam spot size was 5 μm. Oxygen isotopes were measured by peak switching using a Faraday cup for $^{16}O^-$ and an electron multiplier for $^{17}O^-$ and $^{18}O^-$ with a mass resolution of ~5000. The isobaric contribution of $^{16}OH^-$ to $^{17}O^-$ is negligible under these conditions. A typical total count of $^{16}O^-$ in a single analysis was 3 x 10^9 counts. Instrumental mass fractionation and matrix effect were corrected by analyzing terrestrial mineral standards with known isotopic compositions: anorthite, augite, olivine and spinel. Oxygen isotope ratios are expressed in conventional delta notation relative to Standard Mean Ocean Water (SMOW):

$$\delta^{i}O_{SMOW} = [(^{i}O/^{16}O)_{sample}/(^{i}O/^{16}O)_{SMOW} - 1] \times 10^3 \text{ (‰)}, \quad i = 17, 18.$$

Mass-independent enrichment of ^{16}O relative to the SMOW (or the earth) is expressed as $\Delta^{17}O$:

$$\Delta^{17}O = \delta^{17}O_{SMOW} - 0.52 \times \delta^{18}O_{SMOW}.$$

The reported uncertainties of the individual analysis were estimated by taking into account both the internal error of the analysis and the reproducibility of the standard measurements, and are expressed in 2σ. Analyzed spots of a sample were examined by SEM after SIMS analysis to reject any analysis spots that included multi-mineral phases or cracks.

3. RESULTS

3. 1. Petrological observations

WI-025 is an irregularly shaped inclusion with a size of ~2.5 mm x 6 mm easily distinguishable on the sliced Allende slab by its white color. The inclusion consists of three layers with distinct textures and mineral assemblages: the interior portion, igneous rim and an intermediate zone (20 – 300 μm in thickness) that lies between the igneous rim and the interior portion (Fig. 1). The igneous rim is a continuous layer that entirely surrounds the interior portion and the intermediate zone. The thickness of the intermediate zone differs according to location. In some places, the intermediate zone is very thin or is totally absent. The representative chemical compositions of the minerals in each layer are summarized in Table 2.

The interior portion of WI-025 consists of 44% anorthite, 32% spinel, 21% olivine and 2% Al-bearing low-Ca pyroxene in modal composition. Framboidal spinels and olivine granules are distributed throughout the interior portion together with plagioclase (Fig. 2a). Some spinels are surrounded by larger olivine grains. Tiny perovskite grains (~ 0.1 μm) occasionally occur inside the spinel grains. A small amount of tiny Fe sulfides (~ 0.1 μm) are sometimes attached on the spinel grain surfaces.

Most of the spinels are typically 5-15 μm in size and are subhedral in outline with rounded edges. Spinels near the boundary between the interior portion and intermediate zone are much smaller in size. Some spinel grains in direct contact with the intermediate zone show a corroded texture (Fig. 2b). Spinels have a low abundance of Ti (TiO_2 < 0.6 wt.%) and variable abundances of Cr and Fe (Table 2). Chromium shows concentric zonation within a single spinel grain with a Cr_2O_3 abundance ranging from 0.4 wt. % at the center of the grain to 1.7 wt. % at the outermost part of the grain (Fig. 3). The distribution of Fe is decoupled from the distribution of Cr. Most of the spinel grains have a uniformly low Fe concentration of about 0.6 wt. % FeO (Fig. 3). Spinel grains in the outermost part of the interior portion as well as those near cracks have a high Fe abundance of up to 8.6 wt. % FeO. The Fe abundances in the spinels quickly

decrease towards the interior (Fig. 2b).

Olivines in the interior portion are subhedral in outline with irregular surfaces. Some of the olivines occur as lath-like grains. In some areas, the lath-like olivines are locally oriented in same direction (Fig. 2c). Most of the olivines are forsterite with minor concentrations of Fe (0.6-1.7 wt. % FeO). Olivines near the boundary as well as those near cracks have a high Fe concentration of up to 7.8 wt. % FeO.

Al-bearing low-Ca pyroxene occurs as a thin overgrowth (~ 10 μm) on some of the olivine grains (Fig. 2d). It also occurs as separate grains (10 ~ 40 μm) adjacent to olivine at an area near the interior-intermediate zone boundary. The former is relatively Al- and Ti-rich and contains 49.6 - 52.7 wt. % SiO_2, 1.0 - 2.6 wt. % TiO_2, 9.8 - 13.4 wt. % Al_2O_3, 0.5 - 1.2 wt. % Cr_2O_3, < 0.7 wt. % FeO, 32.4 - 34.5 wt. % MgO and 0.2 - 0.6 wt. % CaO (Fig. 4). The later is relatively Ca-rich and contains 54.3 - 57.1 wt. % SiO_2, 0.4 - 0.8 wt. % TiO_2, 2.9 - 6.4 wt. % Al_2O_3, 0.6 - 1.2 wt. % Cr_2O_3, 0.3 - 0.7 wt. % FeO, 34.8 - 36.3 wt. % MgO and 0.9 - 1.3 wt. % CaO (Fig. 4). Anorthite contains minor amounts of Mg (< 0.6 wt. % MgO) and Na (0.3 - 1.5 wt. % Na_2O), with the Na content in the anorthite higher near the interior-intermediate zone boundary and cracks.

The igneous rim is primarily composed of olivine, low-Ca pyroxene and FeS

1 nodules with fine-grained Na-rich feldspathoids and minute amounts of anorthite. The
2 texture and the mineral assemblage of the igneous rim are distinct from that of the
3 interior portion and are analogous with ferromagnesian chondrules. One texture of the
4 igneous rim is characterized by porphyritic olivine occurring within dominant low-Ca
5 pyroxene with minor amount of Fe sulfide blebs (Figs. 5a, b). In Figs. 5a and 5b, olivine
6 and low-Ca pyroxene assemblages (with minor amounts of Fe sulfide and
7 feldspathoids) form clasts of 100 -200 μm in size. One of such clast has spherical
8 outline (Fig. 5b) analogous with chondrules. Fine-grained feldspathoids (nepheline and
9 sodalite) and Fe-rich olivines (~ 23 wt. % FeO) occur interstitially between clasts. The
10 other texture is dominated by porphyritic olivine and Fe sulfide blebs with minor low-Ca
11 pyroxene and feldspathoids (Fig. 5c). Fe sulfides are concentrated at the boundary
12 between the igneous rim and the intermediate portion (Fig. 5d).
13 The olivine phenocrysts are 10 - 60 μm in size and have higher
14 concentrations of Fe (5.2 - 15.8 wt. % FeO) compared to the interior olivines. The
15 outline of olivine phenocrysts is sometimes corroded and Fe-rich layer exists along the
16 outlines and cracks within a grain (Fig. 5a-c). Fine-grained Fe-rich olivines surround
17 olivine phenocrysts (Fig. 5d) and are filling cracks and gaps within and between low-Ca

pyroxene grains (Fig. 5a). The low-Ca pyroxenes are relatively Al-poor compared with the interior pyroxenes and contain 57.3 – 60.0 wt. % SiO_2, < 0.5 wt. % TiO_2, 1.1 – 2.0 wt. % Al_2O_3, 0.4 – 0.6 wt. % Cr_2O_3, 0.6 – 1.0 wt. % FeO, 37.0 – 39.7 wt. % MgO and 0.4 – 0.6 wt. % CaO (Fig. 4).

The intermediate zone is comprised of porphyritic olivine, low-Ca pyroxene and anorthite with fine-grained mesostasis (Fig. 5e, f). Porphyritic grains of olivine, low-Ca pyroxene, anorthite sparsely distribute within fine-grained mesostasis. Fine-grained mesostasis consists of small (< 10 μm in size) Fe-rich olivine (~ 23 wt. % FeO), low-Ca pyroxene, diopside and anorthite with interstitial Na- and Cl-rich feldspathoids and some times show dendritic texture (Fig. 5f). The porphyritic olivines have 3.9 – 9.3 wt. % FeO. Fe-rich layer exists along the outlines and cracks within an olivine phenocryst. Low-Ca pyroxenes occur in two groups with slightly different chemical compositions: one group is chemically similar to the low-Ca pyroxenes in the igneous rim with 53.3 – 57.5 wt. % SiO_2, 0.2 - 0.7 wt. % TiO_2, 1.2 – 7.0 wt. % Al_2O_3, 0.8 – 0.9 wt. % Cr_2O_3, 0.5 – 0.6 wt. % FeO, 36.6 – 37.4 wt. % MgO and 0.3 – 0.4 wt. % CaO, while the other groups has an identical composition to the relatively Ca-rich pyroxenes in the interior portion; 54.2 – 57.5 wt. % SiO_2, 0.3- 0.7 wt. % TiO_2, 1.2 – 7.0 wt. % Al_2O_3,

1 0.7 – 1.7 wt. % Cr_2O_3, 0.5 – 1.0 wt. % FeO, 34.9 – 36.6 wt. % MgO and 0.9 – 1.7 wt. %
2 CaO (Fig. 4).
3
4 **3. 2. Major element abundances**
5 The estimated bulk major element abundances of the interior portion, the
6 igneous rim and the intermediate zone of WI-025 are summarized in Table 3. Each of
7 the three layers has a distinct chemical composition. The interior portion is relatively Ca-
8 and Al-rich while the igneous rim is rich in Fe. The intermediate zone has high Si, Na
9 and Cl abundances and a low Mg abundance in comparison with the other two layers.
10 The igneous rim has major element abundances similar to ferromagnesian
11 chondrules and is plotted within the field of ferromagnesian chondrules defined by
12 chondrules from various carbonaceous and ordinary chondrites in the cosmochemical
13 phase diagram of MacPherson and Huss (2005) (Fig. 6). In the same phase diagram,
14 the interior portion is plotted on the anorthite-saturated side of the spinel-saturated
15 anorthite-forsterite reaction curve, on the Si-saturated side of the thermal divide that sits
16 on the intersection of the anorthite-forsterite reaction curve and the anorthite-forsterite
17 tie line and over the spinel saturation surface (Fig. 6). Therefore, the major element

1 abundances of the interior portion correspond to Al-rich [Plag] chondrules, a subtype of
2 the Al-rich chondrules defined by MacPherson and Huss (2005).
3
4 **3. 3. Trace element abundances**
5 The bulk trace element abundances of the interior portion of WI-025 are
6 summarized in Table 1. Among refractory lithophile REEs, the abundances of light
7 REEs, except for Ce and Eu, are uniformly enriched relative to CI chondrites (9 times
8 the CI chondrite abundance). The abundances of heavy REEs, Ce and Eu are relatively
9 depleted at 0.8 - 6.6 times the abundance of CI chondrites. The overall abundance
10 pattern of REEs is very similar to the group II REE composition of CAIs (Tanaka and
11 Masuda, 1973; Martin and Mason, 1974) and is controlled by the volatility of elements
12 (Fig. 7a). The REE abundance pattern of the WI-025 interior portion, however, has
13 some distinct features compared with that of typical group II CAIs. The abundances of
14 light-REEs are relatively low compared with the typical group II CAIs (20 times the CI
15 chondrite abundance). The La/Lu ratio, which indicates the degree of fractionation
16 between the most refractory Lu and La that have an intermediate volatility among REEs,
17 is relatively small in the WI-025 interior portion. In addition, the degree of Eu anomaly is

relatively small, and a negative Ce anomaly is present.

The abundances of other trace elements are also fractionated based on their volatility. The abundance of super-refractory siderophile Ir is 0.3 times the abundance of CI chondrites. No Re or Os was detected, but the detection limits of 1 and 0.4 x CI indicates that these elements are depleted relative to CI chondrites. Super-refractory lithophile Sc (50%-condensation temperature 1659 K; Lodders, 2003), moderately volatile siderophile Co (50%-condensation temperature 1352 K; Lodders, 2003) and moderately volatile lithophile Cr (50%-condensation temperature 1296 K; Lodders, 2003) are at the CI chondrite level: abundances are 1.5, 0.9 and 1.2 times the CI chondrite abundance for Sc, Co and Cr, respectively. Moderately volatile siderophile Au (50%-condensation temperature 1060 K; Lodders, 2003) and moderately volatile chalcophile Zn (50%-condensation temperature 726 K; Lodders, 2003) are depleted at 0.2 and 0.04 times the abundance of CI chondrites, respectively.

3. 4. Oxygen isotopic compositions

The oxygen isotopic compositions of the minerals in the interior portion, the igneous rim and the intermediate zone of WI-025 are presented in Table 4 and Fig. 8.

Most of the data points, except for anorthites, plot on the Carbonaceous Chondrite Anhydrous Minerals (CCAM) mixing line in the oxygen three-isotope diagram. Oxygen isotopic compositions of the minerals in the interior portion of WI-025 are heterogeneous in terms of ^{16}O enrichment. Spinels are ^{16}O-rich ($\Delta^{17}O$ = -14.2 to -24.7), including a Fe-rich spinel near the boundary that shows $\Delta^{17}O$ = -21.1. The oxygen isotopic compositions of olivines in the interior portion are relatively ^{16}O-poor compared with those of the spinels, and are moderately ^{16}O-rich with a weighted mean $\Delta^{17}O$ value of -6.6 ± 1.3 (2SE, n = 7). No isotopic difference is observed between the lath-like and subhedral olivine grains. The oxygen isotopic compositions of the Al-bearing low-Ca pyroxenes in the interior portion are similar to those of the olivines ($\Delta^{17}O$ = -6.2 ± 0.9; 2SE, n = 7). The weighted mean $\Delta^{17}O$ value of the olivines and Al-bearing low-Ca pyroxenes is -6.3 ± 0.7 (2SE, n = 14). Anorthites in the interior portion are uniformly ^{16}O-poor with a constant $\Delta^{17}O$ value of -2.2 (weighted mean), but show mass-fractionation trending toward the positive $\delta^{18}O$ side of the CCAM line ($\delta^{18}O$ = 9.7 to 16.1).

Anorthite in the igneous rim has similar ^{16}O-poor isotopic compositions ($\Delta^{17}O$ = -2.3) to those of the interior anorthites. Olivines and low-Ca pyroxenes in the igneous

rim are moderately ^{16}O-rich with $\Delta^{17}O$ = -6.1 ± 2.5 (2SE, n = 2) and $\Delta^{17}O$ = -6.0 (n = 1), respectively. Olivines and low-Ca pyroxenes in the intermediate zone are also moderately ^{16}O-rich with average $\Delta^{17}O$ = -6.2 ± 1.6 (2SE, n = 2) and $\Delta^{17}O$ = -5.3 ± 0.9 (2SE, n = 8), respectively. The oxygen isotopic compositions of olivine and low-Ca pyroxene are essentially identical throughout the entire inclusion (Fig. 9).

4. DISCUSSION

4. 1. Origin of the interior portion of WI-025

The interior portion of WI-025 can be categorized as an Al-rich chondrule on the basis of major element chemistry (Fig. 6). However, the interior portion of WI-025 shows several signatures that are characteristic of CAIs. First, the WI-025 interior portion has a bulk REE composition very similar to group II CAIs (Fig. 7a). A highly fractionated group II REE composition is produced only by fractional condensation from a hot gas of solar chemical composition (Boynton, 1975; Davis and Grossman, 1979). Group II CAIs are formed by condensation from a gas that is already condensed out super-refractory elements. Therefore, group II CAIs are depleted in super-refractory trace elements such as Lu, Ho, Dy and PGEs (Kornacki and Fegley, 1986). In the

1 interior portion of WI-025, the abundances of super-refractory PGEs are depleted
2 relative to the CI chondrite abundance (Table 1). This is consistent with the trace
3 element characteristics of group II CAIs. Second, the WI-025 interior portion has a high
4 modal abundance of spinel (32%). Spinel is not a major mineral phase in Al-rich
5 chondrules but is a ubiquitous mineral phase in CAIs. Third, the abundant spinels in the
6 WI-025 interior portion are uniformly ^{16}O-rich (Δ^{17}O = -14.7 to -25.7). Relict spinel grains
7 that show a moderately ^{16}O-rich O isotopic composition (Δ^{17}O from -17 to -10) have
8 been reported previously in ferromagnesian and Al-rich chondrules from Allende and
9 CR chondrites (Maruyama et al., 1999; Maruyama and Yurimoto, 2003; Krot et al.,
10 2006). Oxygen isotopic compositions of such relict spinels are relatively ^{16}O-poor
11 compared to typical CAI spinels (Δ^{17}O ~ -25). On the other hand, the oxygen isotopic
12 compositions of spinels in the interior portion of WI-025 are more ^{16}O-rich and are
13 indistinguishable from those of the CAIs (Fig. 8). These observations indicate that the
14 interior portion of WI-025 contains a CAI component, which was formed by fractional
15 condensation from the solar nebular gas.
16 The interior portion of WI-025 shows a negative Ce anomaly in REE
17 composition (Fig. 7a). Ce is refractory under the reducing conditions generally assumed

in a hot gas of solar composition, but forms a stable gaseous dioxide under oxidizing conditions (Davis et al., 1982). Therefore, the original CAI may have condensed under a high oxygen fugacity environment and become separated from the nebular gas before the Ce was totally condensed to the solid phase.

4. 2. Mixing of CAI and chondrule materials

The interior portion of WI-025 is enriched in Mg and Si compared with CAIs (Table 3). Therefore, closed system re-melting of the precursor CAI material is not sufficient to explain the major element chemistry of the WI-025 interior portion. The difference in major element composition between the WI-025 interior portion and typical CAIs can be simply explained by the assimilation of Mg and Si-rich chondrule material into the original CAI by partial melting. The assimilated material may not actually be a chondrule but a material with chondrule (or chondritic) chemical composition. The major element composition of the WI-025 interior portion is intermediate between those of fine-grained spinel-rich CAIs and ferromagnesian chondrules (Fig. 6), suggesting that the original CAI was a fine-grained spinel-rich CAI, which is plausible as fine-grained spinel-rich CAIs are known to have a group II REE composition.

1

2 **4. 3. Melting conditions of the WI-025 interior portion**

3 The bulk major element composition of the WI-025 interior portion is
4 spinel-saturated; i.e., it plots above the spinel saturation surface in the cosmochemical
5 phase diagram (Fig. 6; MacPherson and Huss, 2005) so that the liquidus-phase mineral
6 is spinel. In equilibrium crystallization, the next mineral to crystallize is anorthite,
7 followed by olivine. Spinel then enters a reaction relationship with the melt when olivine
8 begins to crystallize with anorthite, and lastly cordierite crystallizes. A thermal divide
9 exists on the intersection between the anorthite-forsterite tie-line and
10 spinel-anorthite-olivine reaction curve. Since the interior portion of WI-025 plots on the
11 cordierite side (right hand side) of anorthite-forsterite tie-line (Fig. 6), it will crystallize
12 cordierite rather than diopside. Therefore, the expected mineral assemblage under
13 equilibrium conditions is spinel, anorthite, olivine and cordierite. The interior portion of
14 WI-025 consists of anorthite, spinel, olivine and Al-bearing low-Ca pyroxene. The
15 combination of mineral phases in WI-025 interior is, therefore, inconsistent with that
16 seen in equilibrium crystallization.

17 Tronche et al. (2007) reported a dynamic crystallization experiment for an

Al-rich [Plag] chondrule analog material with a major element composition very similar to that of the WI-025 interior portion (PL2 composition in their study). The reported phase assemblage from the dynamic crystallization experiment using material with this chemical composition was anorthite, spinel, olivine and enstatite. This phase assemblage is slightly different from that expected for equilibrium crystallization, but is in agreement with the mineral assemblage of the WI-025 interior portion. This agreement indicates that the WI-025 interior portion crystallized at a cooling rate fast enough to disturb the equilibrium condition. Tronche et al. (2007) also reported that the textures of product materials of a PL2 composition differ largely depending on the peak heating temperature. When crystallization was started from 1475 ˚C, which is very close to the liquidus temperature of that composition, elongated anorthite phenocrysts or dendritic anorthite dominates the texture. This texture is clearly different from the texture of the interior portion of WI-025 (Fig. 2a). On the other hand, when crystallization was started from the much lower subliquidus temperature of 1416 ˚C, which is still above the temperature at which anorthite first appears (1379 ˚C), the products show a granular texture composed of anorthite, spinel, olivine and enstatite, independent of cooling rate. This texture is analogous with the texture of the interior portion of WI-025

(Fig. 2a).

This similarity in textures suggests that the maximum heating temperature during the melting of the WI-025 interior portion was lower than the liquidus temperature and higher than that at which anorthite first appears. The similarity in major element composition between the WI-025 interior portion and PL2 composition (Tronche et al., 2007) also suggests that the liquidus temperature and that at which anorthite first appears for the WI-025 interior portion are not so different from those for the PL2 composition. Therefore, the maximum heating temperature is probably between 1379 ˚C and 1475 ˚C. Under such melting conditions, melting will be restricted to partial melting and a large portion of the liquidus mineral phase spinel will survive. These melting conditions are consistent with the observation that the ^{16}O-rich spinels have a different oxygen isotopic composition to those of anorthites and olivines (Fig. 8), suggesting that spinels represent a relict phase that had formed in the original CAI.

The maximum heating temperature inferred for the WI-025 interior portion is lower than that of ferromagnesian chondrules, but similar to that of Type-B CAIs. The maximum heating temperatures of igneous Type-B CAIs and ferromagnesian chondrules estimated from crystallization experiments are 1400 ˚C and 1500 ~ 1850 ˚C,

1 respectively (Stolper and Paque, 1986; Jones et al, 2000; Connolly and Burnett, 2003;
2 Connolly et al., 2006; Hewins et al., 2005). The melting of the WI-025 interior portion
3 may have been caused by a similar process to that of melted igneous CAIs rather than
4 that of melted ferromagnesian chondrules.

5 The chemical zoning pattern of the spinel grains also supports the notion that
6 the spinel is a relict left over from partial melting and that chondrule assimilation
7 occurred during the partial melting (Fig. 3). The chemical zoning of Cr in a 10- μm size
8 spinel in the interior portion is concentric within a single grain, with the Cr abundance
9 decreasing toward the interior (Fig. 3). The oxygen isotopic composition of the spinel
10 suggests that the spinel was formed within the original CAI. Cr is a moderately
11 refractory element and is depleted in CAIs: the Cr abundance of typical CAI spinel is
12 very low (< 0.7 wt. % Cr_2O_3; Brearley and Jones, 1998). Chondrule material, on the
13 other hand, contains moderately refractory lithophile elements including Cr, and
14 assimilation of chondrule material into CAI increases the bulk Cr abundance of the
15 inclusion. The Cr zoning pattern of the spinel is consistent with the secondary
16 introduction of Cr from a CAI-chondrule mixture melt into originally Cr-poor spinel during
17 partial melting either by overgrowth of spinel from the melt or by solid-state

1 inter-diffusion of Cr and Al in the spinel. Self-diffusion of oxygen in the spinel is far
2 slower than Cr-Al inter-diffusion: the oxygen self-diffusion coefficient in spinel (Ryerson
3 and McKeegan, 1994) is about two orders of magnitude smaller than the Cr-Al
4 interdiffusion coefficient (Suzuki et al., 2008) at 1400 ˚C. Thus, in either case, the
5 oxygen isotopic composition of the spinel grains, except for the overgrowth portion,
6 retains its original values during the partial melting.
7 Fe is also a moderately refractory element that is depleted in CAIs. Most of
8 the interior spinels are depleted in Fe regardless of their Cr zonation (Fig. 3). There is
9 also a homogeneous Fe distribution within a single grain. Solid-state interdiffusion of
10 Fe-Mg pair is far faster than Cr-Al interdiffusion (Sheng et al., 1992; Liermann and
11 Ganguly, 2002; Suzuki et al., 2008). Therefore, Fe abundances in the spinels are likely
12 to have been homogenized during partial melting and chondrule assimilation. Low Fe
13 abundances suggest that the chondrule material assimilated into WI-025 interior portion
14 was poor in Fe.
15
16 **4. 3. Mixing proportions between CAI and chondrule materials**
17 The REE composition of the WI-025 interior portion is also consistent with the

mixing of CAI and chondrule materials (Fig. 7). REE abundances of the CAI-chondrule mixture can be modeled by simple two-component mixing of CAI and chondrule components, assuming that the CAI component has a typical group II REE composition with LREE abundances 20 times the CI chondrite abundance, and that the chondrule component has an unfractionated REE composition identical to that of CI chondrites. Model REE abundance patterns of CAI-chondrule mixtures with CAI components of 20, 40 and 80 weight % are shown in Fig. 7b together with the assumed REE compositions of the CAI and chondrule components. The REE abundance pattern of the mixture modeled with a 40 weight % CAI component resembles the observed REE abundance pattern of the WI-025 interior portion (Fig. 7). The LREE abundances of the mixture model are lowered to about 9 times the CI chondrite abundance, since the high LREE abundances of the CAI component are diluted by the low LREE abundances of the chondrule component. The La/Lu ratio of the mixture model is smaller than those of group II CAIs because of the relatively low La abundance and the relatively high Lu abundance of the mixture. The degree of Eu anomaly of the mixture model is small compared with those of group II CAIs.

The proportions of the CAI and chondrule components can be quantitatively

estimated from this mixing model. The mean of the La and Sm abundances of the WI-025 interior portion is 9.07 times the CI chondrite abundance. In the model, a CAI-chondrule mixture with a ratio of 42% CAI component to 58% chondrule component by weight shows LREE abundances of 9.07 times the CI chondrite abundance. Thus, the REE composition of the WI-025 interior portion suggests that the interior portion is a mixture of about 40 % (by weight) Group II CAI and 60 % chondrule material.

4. 4. Formation of the igneous rim

The igneous rim of WI-025 has a distinct chemical composition compared with the interior portion. In the cosmochemical phase diagram (Fig. 6), the igneous rim plots within the range of magnesian chondrules alongside with the coarse-grained igneous rims of chondrules from CV3 and LL3 chondrites (Rubin, 1984). The igneous rim is not homogeneous: some part is dominated by low-Ca pyroxene (Fig. 5a) while other part is dominated by olivine (Fig. 5c). Part of the igneous rim is likely to be an aggregate of clasts (Fig. 5a). One clast has a spherical outline suggesting that this clast was a chondrule (Fig. 5b). The igneous rim is, therefore, likely to have formed by accretion of materials with ferromagnesian chondrule-like chemical compositions (some may be

actually chondrules) on to the interior portion. The bulk major element composition of the igneous rim is rich in Fe (Table 3), although some part of Fe in the igneous rim may be introduced by secondary process (section 4.5). The igneous rim contains abundant FeS nodules (Fig. 5a-b), which likely to be Fe metal grains sulfided by secondary process. Therefore, the accreted material that formed the igneous rim is relatively Fe-rich and chemically different from the Fe-poor chondrule material that was assimilated into the interior portion.

The intermediate zone has a chemical composition intermediate between the igneous rim and the interior portion (Fig. 6). Abundant fine-grained mesostasis in the intermediate zone indicates that this region cooled rapidly from a molten state. Olivine and anorthite phenocrysts in the intermediate portion resembles igneous rim olivines and interior anorthites (Fig. 5e). Some interior spinel grains in direct contact with the intermediate zone show a corroded texture (Fig. 2b). These observations suggest that the intermediate zone is a reaction zone where the outermost part of the interior portion reacted with the igneous rim material. The accreted igneous rim material was probably partially molten or hot (close to liquidus temperature) to react with the interior portion, which has lower melting temperature compared with igneous rim material. Because

large part of the interior portion escaped melting and mixing with igneous rim material, the interior portion is likely already cooled and solidified at the time of igneous rim formation.

4.5. Effect of secondary alteration on the parent body

The components of the oxidized CV3 carbonaceous chondrites, including Allende, are affected by secondary Fe-alkali-halogen metasomatism on the parent body (e.g. Krot et al., 1995). Fe-, alkali- and halogen-rich phases such as Fe-rich olivine and feldspathoids are commonly observed in Allende CAIs, chondrules and igneous chondrule rims (e.g. Rubin, 1984; Krot et al., 1995).

The igneous rim of Wi-025, shows textures related to secondary processing on the parent body. Olivine phenocrysts are corroded, surrounded by fine-grained Fe-rich olivines and show Fe-rich layers along outlines and cracks (Fig. 5d). Fine-grained Fe-rich olivines occurring within low-Ca pyroxene grain may have formed by alteration of low-Ca pyroxene (Housely and Cirlin, 1983). Alkali- and halogen-bearing feldspathoids are probably an altered mesostasis. The intermediate zone is dominated by fine-grained feldspathoids and Fe-rich olivine (Fig. 5e-f). High Na and Cl contents of

1 the intermediate zone relative with the igneous rim (Table 3) reflect the high abundance
2 of feldspathoids. These phases are likely to be an alteration product of Al-rich
3 mesostasis. Olivine phenocrysts in the intermediate zone show similar alteration
4 features with rim olivines. These observations shows that the igneous rim and the
5 intermediate zone are largely affected by secondary Fe-alkali-halogen metasomatism
6 on the Allende parent body.

7 The interior portion, on the other hand, has low (< 1 wt. %) abundances of
8 Na_2O, K_2O and FeO (table 3). Secondary phases such as feldspathoids and Fe-rich
9 olivine are rare in the interior portion. A few anorthites that are adjacent to intermediate
10 zone and cracks have slightly high abundance of Na (~ 1.5 wt. % Na_2O). Olivine and
11 spinel are generally Fe-poor. These observations indicate that the effect of secondary
12 process is limited in the interior portion. The interior spinels (and also olivines) that are
13 in contact with the intermediate zone and cracks have relatively high Fe concentrations.
14 The Fe zoning pattern of spinel grains in the interior-intermediate zone boundary (Fig.
15 2b) indicates that introduction of Fe postdates the formation of the interior portion.
16 Introduction of Fe into the interior portion is likely caused by parent body alteration that
17 affected the igneous rim and the intermediate zone. Alternatively, it may be caused by

1 igneous rim formation. The abundant Fe sulfide blebs in the igneous rim indicates that
2 the igneous rim material was originally Fe-rich, although its original feature is obscured
3 by secondary alteration. Diffusion of Fe, provided from the igneous rim material, in
4 spinel and other minerals in the interior portion is likely to have been accelerated by
5 high temperature caused by the addition of the hot igneous rim material.
6
7 **4.6. Environment of the CAI-chondrule mixing**
8 Among the minerals in the WI-025 interior portion, olivine and Al-bearing
9 low-Ca pyroxene did not crystallized from a melt of CAI composition. Olivine and
10 Al-bearing low-Ca pyroxene are crystallized from a melt after the assimilation of
11 chondrule materials. Therefore, the oxygen isotopic compositions of olivine and
12 Al-bearing low-Ca pyroxene in the interior portion ($\Delta^{17}O$ = -6.3) corresponds to the
13 oxygen isotopic composition of the CAI-chondrule mixture melt. If the melting took place
14 in a closed system, the oxygen isotopic composition of the melt is determined by three
15 factors; the oxygen isotopic composition of the original CAI, the oxygen isotopic
16 composition of the assimilated chondrule material and the mixing ratio of the two
17 components. Alternatively, the oxygen isotopic composition of the melt may reflect the

oxygen isotopic composition of the nebular gas at the time of the melting, since isotopic exchange between melt and the surrounding nebular gas is rapid.

Anorthite in the interior portion has a ^{16}O-poor oxygen isotopic composition ($\Delta^{17}O$ = -2.2) that differs from those of olivine and low-Ca pyroxene (Fig. 8). The anorthite may have crystallized from a melt of ^{16}O-poor oxygen isotopic composition. The difference in oxygen isotopic compositions indicates that the melt that crystallized the anorthite is different from the melt that crystallized the olivine and low-Ca pyroxene. Alternatively, the oxygen isotopic composition of the anorthite may have been changed by secondary fluid-assisted alteration on the parent body.

The oxygen isotopic compositions of the olivine and low-Ca pyroxene in both the igneous rim and the intermediate zone are indistinguishable from the oxygen isotopic compositions of the olivine and low-Ca pyroxene in the interior portion (Fig. 9), and the oxygen isotopic compositions of the olivine and low-Ca pyroxene in the interior portion correspond to that of the CAI-chondrule mixture melt. If the oxygen isotopic composition of the CAI-chondrule mixture melt reflects the closed system mixing of CAI and chondrule components, the likelihood of the igneous rim material having an identical oxygen isotopic composition to the CAI-chondrule mixture melt seems to be

very low. Therefore, it is more likely that both the interior portion and the igneous rim melted in the same nebular gas and their oxygen isotopic compositions were buffered to the isotopic composition of the nebular gas. The oxygen isotopic composition of the nebular gas is inferred as $\Delta^{17}O \sim -6.3$. This oxygen isotopic composition is similar to the O isotopic compositions of ferromagnesian chondrules (Chaussidon et al., 2008) as well as to anorthite and melilite in some igneous CAIs (MacPherson, 2003; Yurimoto et al., 2008). During the partial melting of the precursor CAI of the interior portion of WI-025, the partial melt have assimilated chondrule material and increased its mass to about 2.5 times the mass of the precursor CAI. After quick solidification, the interior portion of WI-025 subsequently accumulates multiple chondrule materials that are heated under the same O isotopic composition nebular gas as the interior portion and formed the igneous rim. The original precursor CAI has encountered multiple chondrule materials multiple times within the same O isotopic composition nebular gas. This suggests that the possibility of encountering chondrule material was high in the nebular gas where melting of the WI-025 interior portion and the igneous rim took place. The environment where the melting of the WI-025 interior portion and the igneous rim took place was, therefore, likely rich in chondrule (or chondritic) composition dusts.

1

2 **4.7. Formation conditions of WI-025**

3 WI-025 have underwent at least 2 high-temperature events in the solar nebula
4 prior to incorporation into the Allende parent body. The first high-temperature event is
5 the formation of the precursor CAI of WI-025. The precursor CAI was formed by
6 fractional condensation from a ^{16}O-rich nebular gas. In general, CAIs are considered to
7 have formed at the inner edge of the solar nebula, where the oxygen isotopic
8 composition of the nebular gas is affected by ^{16}O-rich coronal flow of the proto-sun (Itoh
9 and Yurimoto, 2003; Yurimoto et al., 2008). It is very likely that the formation of the
10 precursor CAI of WI-025 took place in such setting together with major CAI populations.
11 The second high-temperature event caused the mixing of CAI and chondrule
12 materials. The precursor CAI was partially melted, assimilated chondrule materials,
13 crystallized the interior portion and formed the igneous rim in same environment. The
14 environment of the nebular gas where this event took place is relatively ^{16}O-poor and
15 chondritic dust-rich. This environment is different from that of the first high-temperature
16 event and suggests that the 2 high-temperature events are spatially and/or temporally
17 separated.

The igneous rim in WI-025 is textually similar to igneous rims of Allende ferromagnesian chondrules suggesting similar conditions of igneous rim formations. The relatively ^{16}O-poor nebular gas ($\Delta^{17}O \sim -6.3$) during the second high-temperature event may suggest that the second high-temperature event is related to the formation of ferromagnesian chondrules. The interior portion crystallized with a cooling rate fast enough to disturb equilibrium crystallization suggesting that the heating was transient. This is consistent with the fast cooling rate inferred for the ferromagnesian chondrules (Jones et al, 2000; Hewins et al., 2005; Connolly et al., 2006). However, the maximum heating temperature of the second event inferred from the texture of the interior portion of WI-025 is 1379-1475 ˚C, which is lower than the maximum heating temperature inferred for ferromagnesian chondrules (Jones et al, 2000; Hewins et al., 2005; Connolly et al., 2006). Therefore, the nature of the heating in the second high-temperature event seems to be slightly different from the condition inferred for chondrule heating.

Alternatively, the second high-temperature event may be related to melting of CAIs. The inferred maximum heating temperature of the second event is consistent with the maximum heating temperature of the igneous CAIs (Stolper and Paque, 1986;

Jones et al, 2000; Connolly and Burnett, 2003). High-temperature processing of CAIs occurred not only in ^{16}O-rich nebular gas but also in ^{16}O-poor nebular gas. Yurimoto et al. (1998) showed that a type-B CAI from Allende have melted partially in a ^{16}O-poor nebular gas. Park et al. (2012) showed that melilite crystals in a gehlenitic mantle of a Type A from Allende are condensed from a nebular gas changing from ^{16}O-poor to ^{16}O-rich. These findings show that some CAIs underwent high-temperature processing in a ^{16}O-poor nebular gas. Therefore, ^{16}O-poor oxygen isotopic composition may not be sufficient to reject the idea that the second high-temperature event is related to melting of CAIs. Timing of the second high-temperature event may be an important factor to distinguish if the second high-temperature event is related to melting of CAIs or not.

5. CONCLUSION

WI-025 is a compound object consisting of an interior portion, which is chemically comparable to an Al-rich [plag] chondrule, and a ferromagnesian chondrule-like igneous rim. Several lines of evidence indicate that the interior portion is a CAI-chondrule hybrid. The interior portion of WI-025 was originally formed as a CAI before later assimilating chondrule material. The results indicate the existence of a

heating event in the solar nebula that melted both the CAI and chondrule materials under melting conditions similar to the melting of igneous CAIs. The inclusion formed through multiple heating episodes in different nebular gases with different oxygen isotopic compositions. The formation history of WI-025 can be summarized in 3 stages as follows: 1) original CAI formation, 2) partial melting and assimilation of chondrule material, 3) igneous rim formation and 4) secondary alteration on the parent body.

Stage 1: WI-025 was originally formed as a CAI by fractional condensation in a ^{16}O-rich environment. The original CAI had a group II REE composition and might have existed as a fine-grained spinel-rich CAI. Condensation of the original CAI with a negative Ce anomaly may have occurred under a high oxygen fugacity environment. The ^{16}O-rich spinels in the WI-025 interior portion were formed in this stage.

Stage 2: The original CAI was partially melted in a moderately ^{16}O-poor nebular gas (Δ^{17}O ~ -6.3) and ferromagnesian chondrule material was assimilated. The maximum heating temperature of the partial melting is estimated as about 1400 ˚C (1379 ˚C - 1475 ˚C). This is similar to the melting temperature of igneous CAIs. The mixing ratio of the original CAI and assimilated chondrule material is estimated as about 40% CAI (by weight) to 60% chondrule material. Minerals in the interior portion, other

than spinel, were crystallized in this stage. Cr was introduced into WI-025 from the chondrule component and formed a Cr chemical zoning of spinel either by overgrowth of Cr-rich spinel or solid-state diffusion.

Stage 3: After solidification of the interior portion, Fe-rich chondrule materials, which melted in a moderately ^{16}O-poor nebular gas ($\Delta^{17}O \sim -6.6$), accreted to the interior portion and formed the igneous rim. The chemical composition of these chondrule materials are different from the Fe-poor chondrule material that was assimilated into the interior portion. Some portion of the melted chondrule material reacted with the outermost part of the interior portion and formed the intermediate zone.

Stage 4: After formation of the igneous rim and incorporation into the Allende parent body, the inclusion underwent secondary Fe-alkali-halogen metasomatic alteration on the parent body. Feldspathoids and Fe-rich olivine in the igneous rim and the intermediate portion are products of the alteration.

Acknowledgments. We are grateful to M. Minami and S. Shibata for their help with the INAA analysis, to S. Yoshioka for preparation of the silica tubes used in the INAA analysis, and to K. Abe for his technical assistance with the SEM-EDS analysis. We

would like to thank J. C. Bridges, A. E. Rubin and S. S. Russell for their detailed and helpful reviews that greatly improved the quality of the manuscript. This work was supported by KAKENHI.

REFERENCES

Amelin Y. and Krot A. (2007) Pb isotopic age of the Allende chondrules. *Meteorit. Planet. Sci.* **42**, 1321-1335.

Amelin Y., Kaltenbach A., Iizuka T., Stirling C. H., Ireland T. R., Petaev M. and Jacobsen S. B. (2010) U-Pb chronology of the Solar system's oldest solids with variable $^{238}U/^{235}U$. *Earth Planet. Sci. Lett.* **300**, 343-350.

Amelin Y., Krot A. N., Hutcheon I. D. and Ulyanov A. A. (2002) Lead isotopic ages of chondrules and calcium-aluminum-rich inclusions. *Science* **297**, 1678-1683.

Bischoff A. and Keil K. (1984) Al-rich objects in ordinary chondrites: Related origin of carbonaceous and ordinary chondrites and their constituents. *Geochim. Cosmochim. Acta* **48**, 693-709.

Bischoff A., Palme H. and Spettel B. (1989) Al-rich chondrules from the Ybbsitz H4-chondrite: evidence for formation by collision and splashing. *Earth Planet. Sci.*

Lett. **93**, 170-180.

Bouvier A., Blichert-Toft J., Moynier F., Vervoort J. D. and Albarède F. (2007) Pb-Pb dating constraints on the accretion and cooling history of chondrites. *Geochim. Cosmochim. Acta* **71**, 1583-1604.

Boynton W. V. (1975) Fractionation in the solar nebula: condensation of yttrium and the rare earth elements. *Geochim. Cosmochim. Acta* **39**, 569-584.

Brearley A. J. and Jones R. H. (1998) Chondritic Meteorites. In *Reviews in Mineralogy Vol. 36 Planetary Materials* (ed. Papike J. J.), Mineralogical Society of America, Washington D. C., pp. 3-1-3-398

Bridges J. C., Franchi I. A., Hutchison R., Sexton A. S. and Pillinger C. T. (1998) Correlated mineralogy, chemical compositions, oxygen isotopic compositions and size of chondrules. *Earth Planet. Sci. Lett.* **155**, 183-196.

Chaussidon M., Libourel G. and Krot A. N. (2008) Oxygen isotopic constraints on the origin of magnesian chondrules and on the gaseous reservoirs in the early solar system. *Geochim. Cosmochim. Acta* **72**, 1924-1938.

Connolly H. C. Jr. and Burnett D. S. (2003) On type B CAI formation: Experimental constraints on fO_2 variations in spinel minor element partitioning and reequilibration

effects. *Geochim. Cosmochim. Acta* **67**, 4429-4434.

Connolly H. C. Jr., Desch S. J., Ash R. D. and Jones R. H. (2006) Transient heating events in the protoplanetary Nebula. In *Meteorites and the Early Solar System II* (eds. Lauretta D. S. and McSween H. Y.), the University of Arizona, Tucson, pp. 383-398.

Connelly J. N., Amelin Y., Krot A. N. and Bizarro M. (2008) Chronology of the solar system's oldest solids. *Astrophys. J.* **375**, L121-L124.

Davis A. M. and Grossman L. (1979) Condensation and fractionation of rare earths in the solar nebula. *Geochim. Cosmochim. Acta* **43**, 1611-1632.

Davis A. M., Tanaka T., Grossman L., Lee T. and Wasserburg G. J. (1982) Chemical composition of HAL, an isotopically-unusual Allende inclusion. *Geochim. Cosmochim. Acta* **46**, 1627-1651.

Dodd R. T. (1978) Compositions of droplet chondrules in the Manych (L-3) chondrite and the origin of chondrules *Earth Planet. Sci. Lett.* **40**, 71-82.

Ebel D. S., Weisberg M. K., Hertz J. and Campbell A. J. (2008) Shape, metal abundance, chemistry, and origin of chondrules in the Renazzo (CR) chondrite. *Meteorit. Planet. Sci.* **43**, 1725-1740.

Evensen N. M., Carter S. R., Hamilton P. J., O'Nions R. K. and Ridley W. I. (1979) A combined chemical-petrological study of separated chondrules from the Richardton meteorite. *Earth Planet. Sci. Lett.* **42**, 223-236.

Grossman L. and Ganapathy R. (1976) Trace elements in the Allende meteorite – I. Coarse-grained, Ca-rich inclusions. *Geochim. Cosmochim. Acta* **40**, 331-344.

Grossman L., Ganapathy R. and Davis A. M. (1977) Trace elements in the Allende meteorite – III. Coarse-grained inclusions revisited. *Geochim. Cosmochim. Acta* **41**, 1647-1664.

Grossman J. N., Rubin A. E., Rambaldi E. R., Rajan R. S. and Wasson J. T. (1985) Chondrules in the Qingzhen type-3 enstatite chondrite: Possible precursor components and comparison to ordinary chondrite chondrules. *Geochim. Cosmochim. Acta* **49**, 1781-1795.

Hewins R. H., Connoly H. C. Jr., Lofgren G. E. and Libourel G. (2005) Experimental constraints on chondrule formation. In *Chondrites and the Protoplanetary Disk* (eds. Krot A. N., Scott E. R. D. and Reipurth B.), Astronomical Society of the Pacific, San Francisco, pp.286-316.

Huang S., Lu J., Prinz M., Weisberg M. K., Benoit P. H. and Sears D. W. G. (1996)

Chondrules: Their diversity and the role of open-system processes during their formation. *Icarus* **122**, 316-346.

Itoh S. and Yurimoto H. (2003) Contemporaneous formation of chondrules and refractory inclusions in the early solar system. *Nature* **423**, 728-731.

Jacobsen B., Yin Q., Moynier F., Amelin Y., Krot A. N., Nagashima K., Hatcheon I. D. and Palme H. (2008) ^{26}Al-^{26}Mg and ^{207}Pb-^{206}Pb systematics of Allende CAIs: Canonical solar initial 26Al/27Al ratio reinstated. *Earth Planet. Sci. Lett.* **272**, 353-364.

Jones R. H. (1990) Petrology and mineralogy of Type II, FeO-rich chondrules in Semarkona (LL3.0): Origin by closed-system fractional crystallization, with evidence for supercooling. *Geochim. Cosmochim. Acta* **54**, 1785-1802.

Jones R. H. (1994) Petrology of FeO-poor, porphyritic pyroxene chondrules in the Semarkona chondrite. *Geochim. Cosmochim. Acta* **58**, 5325-5340.

Jones R. H. and Scott E. R. D. (1989) Petrology and thermal history of type IA chondrules in the Semarkona (LL3.0) Chondrite. *Proc. 19th Lunar Planet. Sci. Conference,* 523-536.

Jones R. H., Lee T., Connolly H. C. Jr., Love S. G. and Shang H. (2000) Formation of

chondrules and CAIs: theory vs. observation. In *Protostars and Planets IV* (eds. Mannings V., Boss A. P. and Russell S. S.), University of Arizona Press, Tucson, pp. 927-962.

Kita N. T., Huss G. R., Tachibana S., Amelin Y., Nyquist L. E. and Hutcheon I. D. (2005) Constraints on the origin of chondrules and CAIs from Short-lived and long-lived radionuclides. . In *Chondrites and the Protoplanetary Disk* (eds. Krot A. N., Scott E. R. D. and Reipurth B.), Astronomical Society of the Pacific, San Francisco, pp.558-587.

Kornacki A. S. and Fegley, Jr. B. (1986) The abundance and relative volatility of refractory trace elements in Allende Ca, Al-rich inclusions: implications for chemical and physical processes in the solar nebula, *Earth Planet. Sci. Lett.* **79**, 217-234.

Krot A. N. and Rubin A. E. (1994) Glass-rich chondrules in ordinary chondrites. *Meteoritics* **29**, 697-707.

Krot A. N., Scott E. R. D. and Zolensky M. E. (1995) Mineralogical and chemical modification of components in CV3 chondrites: Nebular or asteroidal processing? *Meteoritics* **30**, 748-775.

Krot A. N., McKeegan K. D., Russell S. S., Meibom A., Weisberg M. K., Zipfel J., Krot T.

V., Fagan T. J. and Keil K. (2001) Refractory calcium-aluminum-rich inclusions and aluminum-diopside-rich chondrules in the metal-rich chondrites Hammadah al Hamra 237 and Queen Alexandra Range 94411. *Meteorit. Planet. Sci.* **36**, 1189-1216.

Krot A. N., MacPherson G. J., Ulyanov A. A., and Petaev M. I. (2004) Fine-grained, spinel-rich inclusions from the reduced CV chondrites Efremovka and Leoville: I. Mineralogy, petrology, and bulk chemistry. *Meteorit. Planet. Sci.* **39**, 1517-1553.

Krot A. N., Yurimoto H., Hutcheon I. MacPherson G. J. (2005) Chronology of the early solar system from chondrule-bearing calcium-aluminum-rich inclusions. *Nature* **434**, 998-1001.

Krot A. N., Libourel G. and Chaussidon M. (2006) Oxygen isotope compositions of chondrules in CR chondrites. *Geochim. Cosmochim. Acta* **70**, 767-779.

Krot A. N., Chaussidon M., Yurimoto H., Sakamoto N., Nagashima K., Hutcheon I. D. and MacPherson G. J. (2008) Oxygen isotopic compositions of Allende Type C CAIs: Evidence for isotopic exchange during nebular melting and asteroidal metamorphism. *Geochim. Cosmochim. Acta* **72**, 2534-2555.

Liermann H. P. and Ganguly J. (2002) Diffusion kinetics of Fe^{2+} and Mg in aluminous

spinel: Experimental determination and applications. *Geochim. Cosmochim. Acta* **66**, 2903-2913.

Lodders K. (2003) Solar system abundances and condensation temperatures of the elements. *Astrophys. J.* **591**, 1220-1247.

MacPherson G. J. (2003) Calcium-aluminum-rich inclusions in chondritic meteorites. In *Meteorites, Comets, and Planets* (ed. A. M. Davis) *Vol. 1 Treatise on Geochemistry* (eds, H. D. Holland and K. K. Turekian), Elsevier-Pergamon, Oxford, pp. 201-246.

MacPherson G. J. and Huss G. R. (2005) Petrogenesis of Al-rich chondrules: Evidence from bulk compositions and phase equilibria. *Geochim. Cosmochim. Acta* **69**, 3099-3127.

MacPherson G. J., Davis A. M. and Zinner E. K. (1995) The distribution of aluminum-26 in the early solar system – a reappraisal. *Meteoritics* **30**, 365-386.

Martin P. M. and Mason B. (1974) Major and trace elements in the Allende meteorite. *Nature* **249**, 333-334.

Maruyama S. and Yurimoto H. (2003) Relationship among O, Mg isotopes and the petrography of two spinel-bearing compound chondrules. *Geochim. Cosmochim. Acta* **67**, 3943-3957.

Maruyama S., Yurimoto H. and Sueno S. (1999) Oxygen isotopic evidence regarding the formation of spinel-bearing chondrules. *Earth Planet. Sci. Lett.* **169**, 165-171.

Mason B. and Martin P. M. (1974) Minor and trace element distribution in melilite and pyroxene from the Allende meteorite. *Earth Planet. Sci. Lett.* **22**, 141-144.

Mason B. and Martin P. M (1977) Geochemical differences among components of the Allende meteorite. *Smithson. Contrib. Earth Sci.* **19**, 84-95.

Mason B. and Taylor S. R. (1982) Inclusions in the Allende meteorite. *Smithson. Contrib. Earth Sci.* **25**, 1-30.

McCoy T. J., Scott E. R. D., Jones R. H., Keil K. and Taylor G. J. (1991) Composition of chondrule silicates in LL3-5 chondrites and implications for their nebular history and parent body metamorphism. *Geochim. Cosmochim. Acta* **55**, 601-619.

Misawa K. and Fujita T. (1994) A relict refractory inclusion in a ferromagnesian chondrule from the Allende meteorite. *Nature* **368**, 723-726.

Misawa K. and Nakamura N. (1988) Highly fractionated rare-earth elements in ferromagnesian chondrules from the Felix (CO3) meteorite. *Nature* **334**, 47-50.

Nagahara H. and Kushiro I. (1982) Calcium-Aluminum-rich chondrules in the unequilibrated ordinary chondrites. *Meteoritics* **17**, 55-63.

Nagahara H., Kita N. T., Ozawa K. and Morishita Y. (2009) Condensation of major elements during chondrule formation and its implication to the origin of chondrules. *Geochim. Cosmochim. Acta* **72**, 1442-1465.

Nakamura N., Misawa K., Kitamura M., Masuda A., Watanabe S. and Yamamoto K. (1990) Highly fractionated REE in the Hedjaz (L) chondrite: implications for nebular and planetary processes. *Earth Planet. Sci. Lett.* **99**, 290-302.

Park C., Wakaki S., Sakamoto N., Kobayashi S. and Yurimoto H. (2012)_Oxygen isotopic composition of the solar nebular gas inferred from high precision isotope imaging of melilite crystals in an Allende CAI. *Meteorit. Planet. Sci.,* submitted.

Rout S. S., Keil K. and Biscoff A. (2010) Bulk chemical compositions of Al-rich objects from Rumuruti (R) chondrites: implications for their origin. *Chemie der Erde* **70**, 35-53.

Rubin A. E. (1982) Coarse-grained chondrule rims in type 3 chondrites. *Geochim. Cosmochim. Acta* **48**, 1779-1789.

Rubin A. E. and Wasson J. T. (1987a) Chondrules, matrix and coarse-grained chondrule rims in the Allende meteorite: Origin, interrelationships and possible precursor components. *Geochim. Cosmochim. Acta* **51**, 1923-1937.

Rubin A. E. and Wasson J. T. (1987b) Chondrules in the Murray CM2 meteorite and compositional differences between CM-CO and ordinary chondrite chondrules. *Geochim. Cosmochim. Acta* **50**, 307-315.

Rubin A. E. and Wasson J. T. (1988) Chondrules and matrix in the Ornans CO3 meteorite: Possible precursor components. *Geochim. Cosmochim. Acta* **52**, 425-432.

Ruzicka A., Snyder G. A. and Taylor L. A. (1998) Mega-chondrules and large, igneous-textured clasts in Julesberg (L3) and other ordinary chondrites: Vapor-fractionation, shock-melting, and chondrule formation. *Geochim. Cosmochim. Acta* **62**, 1419-1442.

Ryerson F. J. and McKeegan K. D. (1994) Determination of oxygen self-diffusion in åkermanite, anorthite, diopside, and spinel: Implications for oxygen isotopic anomalies and the thermal histories of Ca-Al-rich inclusions. *Geochim. Cosmochim. Acta* **58**, 3713-3734.

Scott E. R. D. and Krot A. N. (2005) Chondritic meteorites and the high-temperature nebular origins of their components. In *Chondrites and the Protoplanetary Disk* (eds. Krot A. N., Scott E. R. D. and Reipurth B.), Astronomical Society of the Pacific, San

Francisco, pp.15-53.

Sears D. W. G. and Sparks M. H. (1984) Chemical and physical studies of type 3 chondrites -III. Chondrules from the Dhajala H3.8 chondrite. *Geochim. Cosmochim. Acta* **48**, 1189-1200.

Sheng Y. J., Hutcheon I. D. and Wasserburg G. J. (1991) Origin of plagioclase-olivine inclusions in carbonaceous chondrites. *Geochim. Cosmochim. Acta* **55**, 581-599.

Sheng Y. J., Wasserburg G. J. and Hutcheon I. D. (1992) Self-diffusion of magnesium in spinel and in equilibrium melts: Constraints on flash heating of silicates. *Geochim. Cosmochim. Acta* **56**, 2535-2546.

Srinivasan G., Huss G. R. and Wasserburg G. J. (2000) A petrographic, chemical, and isotopic study of calcium-aluminum-rich inclusions and aluminum-rich chondrules from the Axtell (CV3) chondrite. *Meteorit. Planet. Sci.* **35**, 1333-1354.

Stolper E. and Paque J. M. (1986) Crystallization sequences of Ca-Al-rich inclusions from Allende: The effects of cooling rate and maximum temperature *Geochim. Cosmochim. Acta* **50**, 1785-1806.

Suzuki A. M., Yasuda A. and Ozawa K. (2008) Cr and Al diffusion in chromite spinel: experimental determination and its implication for diffusion creep. *Phys. Chem.*

Minerals **35**, 433-445.

Sylvester P. J., Grossman L. and MacPherson G. J. (1992) Refractory inclusions with unusual chemical compositions from the Vigarano carbonaceous chondrite. *Geochim. Cosmochim. Acta* **56**, 1343-1365.

Tanaka T. and Masuda A. (1973) Rare-earth elements in matrix, inclusions, and chondrules of the Allende meteorite. *Icarus* **19**, 523-530.

Tronche E. J., Hewins R. H. and MacPherson G. J. (2007) Formation conditions of aluminum-rich chondrules. *Geochim. Cosmochim. Acta* **71**, 3361-3381.

Villeneuve J., Chaussidon M. and Libourel G. (2009) Homogeneous distribution of ^{26}Al in the solar system from the Mg isotopic composition of chondrules. *Science* **325**, 985-988.

Wark D. A. (1987) Plagioclase-rich inclusions in carbonaceous chondrite meteorites: Liquid condensates? *Geochim. Cosmochim. Acta* **51**, 221-242.

Wark D. A. and Lovering J. F. (1982) The nature and origin of type B1 and B2 Ca-Al-rich inclusions in the Allende meteorite. *Geochim. Cosmochim. Acta* **46**, 2581-2594.

Yurimoto H., Ito M. and Nagasawa H. (1998) Oxygen isotope exchange between refractory inclusion in Allende and solar nebula gas. *Science* **282**, 1874-1877.

Yurimoto H., Krot A. N., Choi B. -G., Aleon J., Kunihiro T. and Brearley A. J. (2008) Oxygen isotopes of chondritic components. In *Reviews in Mineralogy and Geochemistry Vol. 68 Oxygen in the solar system* (eds. MacPherson G. J., Mittlefehldt D. W., Jones J. H. and Simon S. B.), Mineralogical Society of America, Washington D. C., pp.141-186

FIGURE CAPTIONS

Fig. 1 A back-scattered electron (BSE) image of WI-025 from Allende chondrite showing the irregular shape of the inclusion. Boundaries between the interior portion, the igneous rim and the intermediate zone, shown as white broken lines, are irregularly shaped. The numerous white colored minerals observed in the igneous rim are FeS. The outlined regions are shown in detail in Figs. 2 and 5.

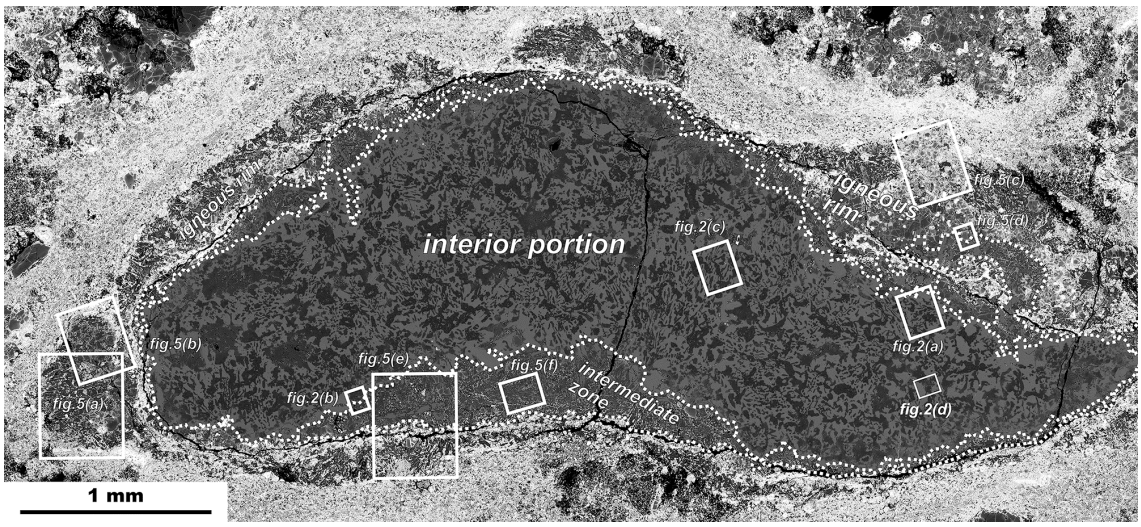

Fig. 2 BSE images of the interior portion of WI-025. a) The interior portion showing an igneous texture where olivine and anorthite fill the spaces between spinel grains. The outlined region is shown in Fig. 3. b) The boundary area between the interior portion and the intermediate zone. The boundary is shown as white broken lines. The interior portion (left hand side) and the intermediate zone (right hand side) are clearly

distinguishable by the differences in texture. Color gradations of the spinel grains in the interior portion reflect the difference in Fe content: Spinels close to the intermediate zone have a higher Fe content. Spinels that are in contact with the intermediate zone are small and show a corroded texture. The irregularly shaped phase (light gray) in the intermediate zone is Fe-rich olivine. c) The interior portion showing locally oriented lath-like olivines (left hand side). d) The interior portion showing an Al-bearing low-Ca pyroxene texture. Abbreviations: an, anorthite; nep, nepheline; ol, olivine; px, low-Ca pyroxene; sp, spinel.

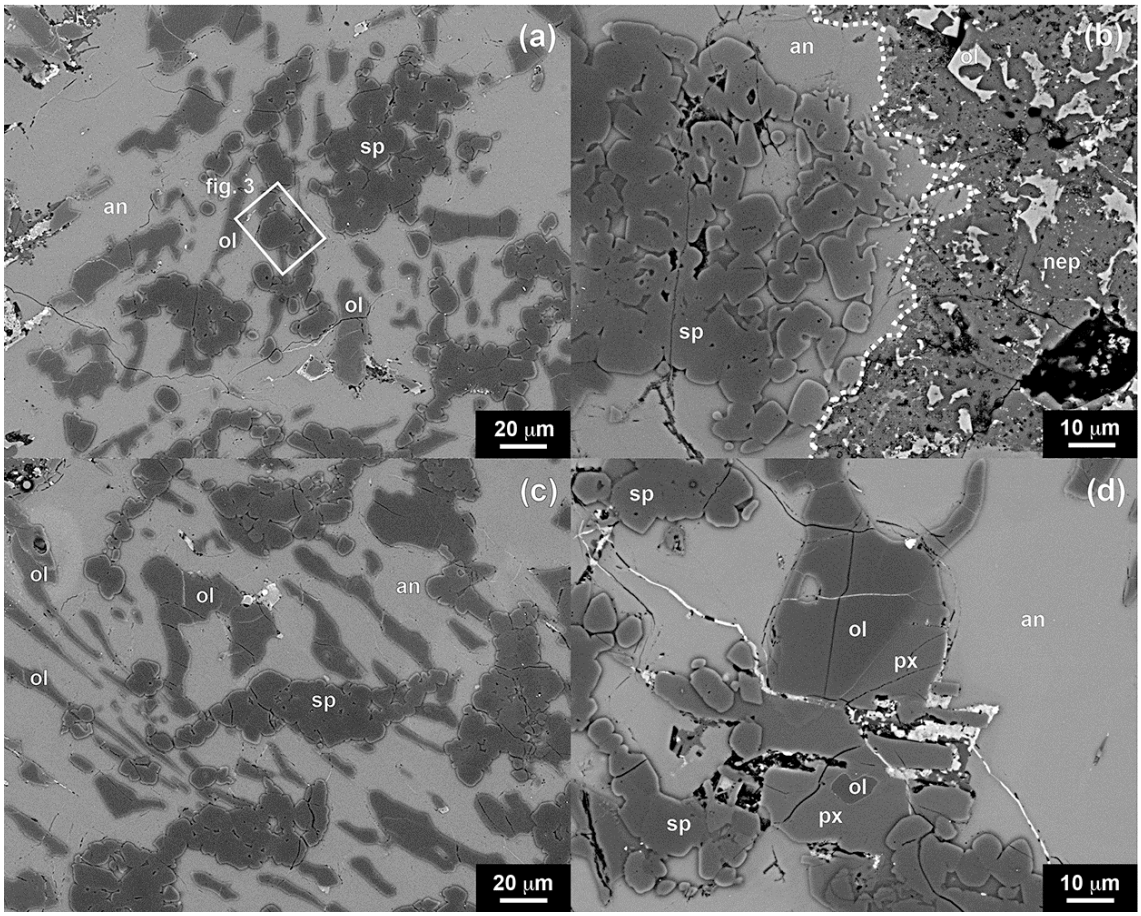

Fig. 3 Close-up images of a spinel grain in the interior portion of WI-025. a) A BSE image of the region outlined in Fig. 2a. The bright edges of the spinel grains may represent a polishing effect. b) X-ray intensity map for Cr. The spinel grain in the center shows concentric Cr zoning with a Cr-poor interior. Smaller spinel grains are uniformly enriched in Cr. c) X-ray intensity map for Ca. The bright areas in the spinel grain in the center may due to an unidentified inclusion or a depth effect of the EDS analysis. d) X-ray intensity map for Fe. In contrast to the Cr zoning pattern, Fe in the spinel grains is uniformly distributed and does not show any chemical zoning. Abbreviations: an, anorthite; ol, olivine; sp, spinel.

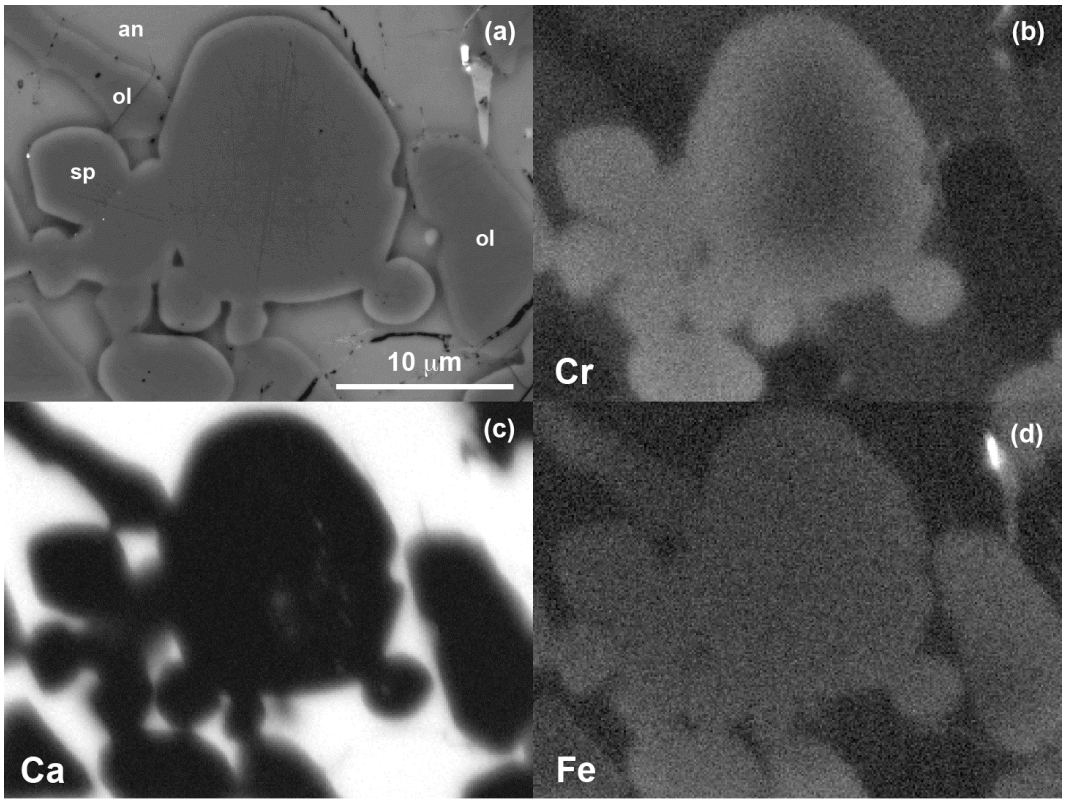

Fig. 4 Chemical compositions of low-Ca pyroxene of WI-025: (a) CaO wt.% and (B) TiO_2 wt. % of the low-Ca pyroxenes from the interior portion (black circle), the igneous rim (white diamond) and the intermediate zone (gray triangle) are plotted against Al_2O_3 wt. %. Some of the low-Ca pyroxenes in the interior portion are in direct contact with the intermediate zone.

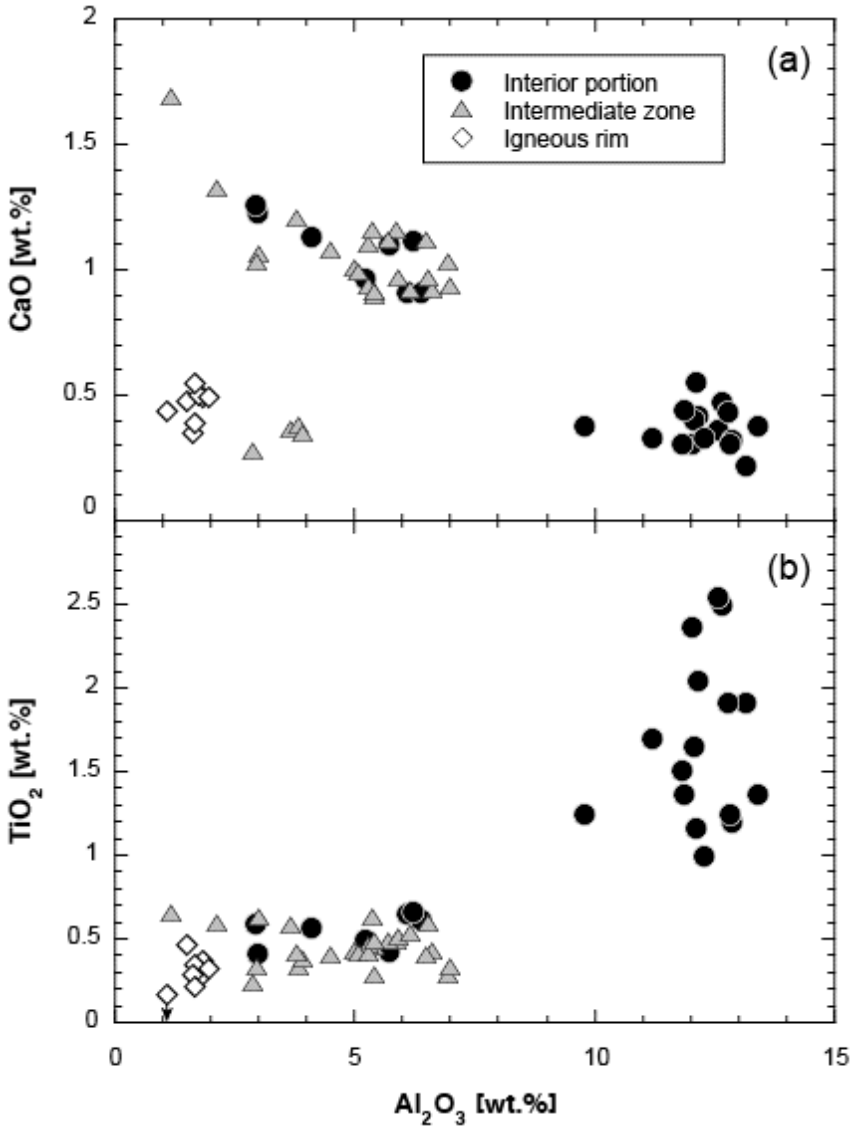

Fig. 5 BSE images of the igneous rim and the intermediate portion of WI-025.

a) Texture of the igneous rim showing multiple olivine-pyroxene clasts (e.g. upper center). Fine-grained feldspathoids (nepheline and sodalite) and ferrous olivine are filling the space between clasts. Fe-sulfide occurs as spherical blebs. Fine-grained Fe-rich olivine (light gray phase) surrounds olivine phenocrysts and fill cracks within low-Ca pyroxene grains. The igneous rim is in direct contact with the surrounding matrix (left hand side). b) An olivine-pyroxene clast in the igneous rim with a spherical shape analogous with chondrules. Mesostasis-like nepheline occurs interstitially among elongated olivine grains and low-Ca pyroxene blocks. Fe sulfide nodule is absent in this clast. Left part of the clast is in contact with the matrix. c) A portion of the igneous rim is dominated by porphyritic olivine grains with abundant Fe sulfide blebs. d) Olivine phenocryst at the igneous rim intermediate zone boundary. The outline of the olivine phenocryst is corroded and, in some place, replaced by fine-grained Fe-rich olivine. e) Texture of the boundary between the igneous rim (left) and the intermediate zone (right). Fe sulfide blebs in the igneous rim are concentrated at the boundary (center). In the intermediate zone, phenocrysts of anorthite, olivine and low-Ca pyroxene, each of which have corroded surface, are sparsely distributes among the fine-grained mesostasis. f) Fine-grained mesostasis in the intermediate zone. Fine-grained

mesostasis consists of Fe-rich olivine, low-Ca pyroxene, diopside and anorthite with interstitial nepheline and sodalite. Some minerals are dendritic and facing the same direction. The bright phase that crosses the upper part of the image consists of Fe and S and is probably Fe Sulfide vein. Abbreviations: an, anorthite; FeS, Fe sulfide; nep, nepheline; ol, olivine; px, low-Ca pyroxene; sp, spinel.

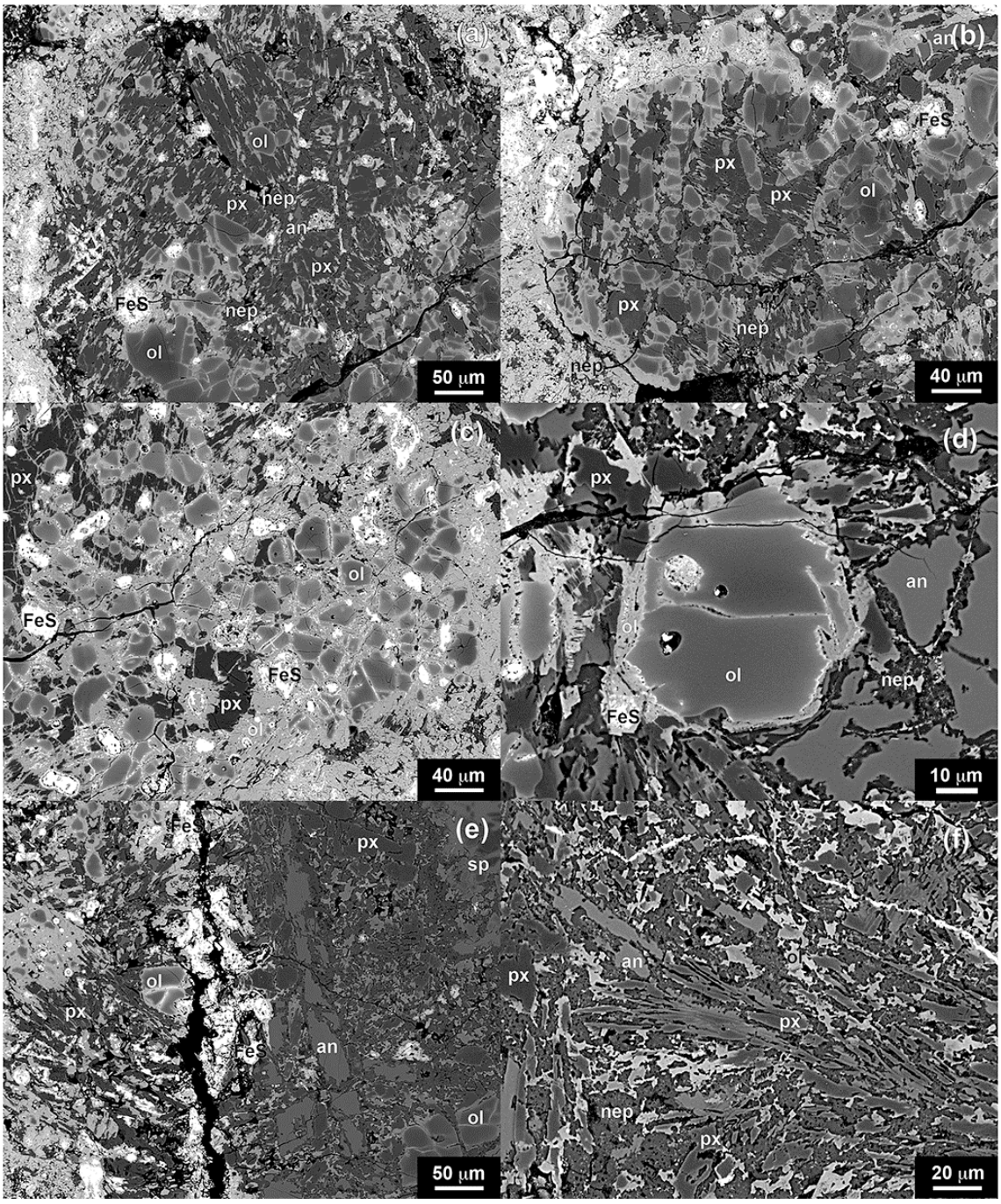
(a)
ol
px
nep
an
px
FeS
nep
ol
50 μm
(b)
an
FeS
px
px
ol
px
nep
nep
40 μm
(c)
px
ol
FeS
FeS
px
ol
40 μm
(d)
px
an
ol
ol
nep
FeS
10 μm
(e)
FeS
px
sp
ol
px
FeS
an
ol
50 μm
(f)
an
ol
px
px
nep
px
20 μm

1

2

3

4

Fig. 6 Bulk major element abundances of the interior portion (black circle), the igneous rim (white diamond) and the intermediate zone (gray triangle) of WI-025 projected from spinel ($MgAl_2O_4$) onto the plane Ca_2SiO_4-Forsterite (Mg_2SiO_4)-Corundum (Al2O3) (cosmochemical phase diagram: MacPherson and Huss, 2005). Literature data of fine-grained CAIs (cross: Mason and Taylor, 1982; Sylvester et al., 1992; and Krot et al., 2004) and coarse-grained igneous rims of chondrules (white square: Rubin, 1984) are plotted as a reference. Boundary curves show the spinel-saturated phase equilibrium of the liquidus-phase minerals. The bulk major element composition of the interior portion plots above the spinel saturation surface in this figure and, thus, is saturated in spinel. Therefore, spinel-saturated boundary curves are valid for discussing the phase relationship of the interior portion. However, bulk major element compositions of the igneous rim and the intermediate zone are under-saturated in spinel, and the spinel-saturated boundary curves are not valid for these two portions. The thin dotted line represents the forsterite-anorthite tie-line. The bulk major element abundance fields of magnesian chondrules, Al-rich chondrules and igneous CAIs (Type A, B and C) plotted in the figure are defined based on data from Bischoff and Keil (1984), Bischoff et al. (1989), Bridges et al. (1998), Dodd (1978), Ebel et al. (2008), Evensen et al. (1979),

Grossman and Ganapathy (1976), Grossman et al. (1977), Grossman et al. (1985), Huang et al. (1996), Jones (1990), Jones (1994), Jones and Scott (1989), Krot and Rubin (1994), Krot et al. (2001), MacPherson and Huss (2005), Mason and Martin (1974), Mason and Martin (1977), Mason and Taylor (1982), McCoy et al. (1991), Nagahara and Kushiro (1982), Nagahara et al. (2009), Nakamura et al. (1990), Rout et al. (2010), Rubin and Wasson (1987a), Rubin and Wasson (1987b), Rubin and Wasson (1988), Ruzicka et al. (1998), Sears and Sparks (1984), Srinivasan et al. (2000), Sylvester et al. (1992), Wark (1987) and Wark and Lovering (1982). Abbreviations: An, anorthite; Cor, corundum; Di, diopside; En, enstatite; Fo, forsterite; Geh, gehlenite; Hib, hibonite; Mel, melilite.

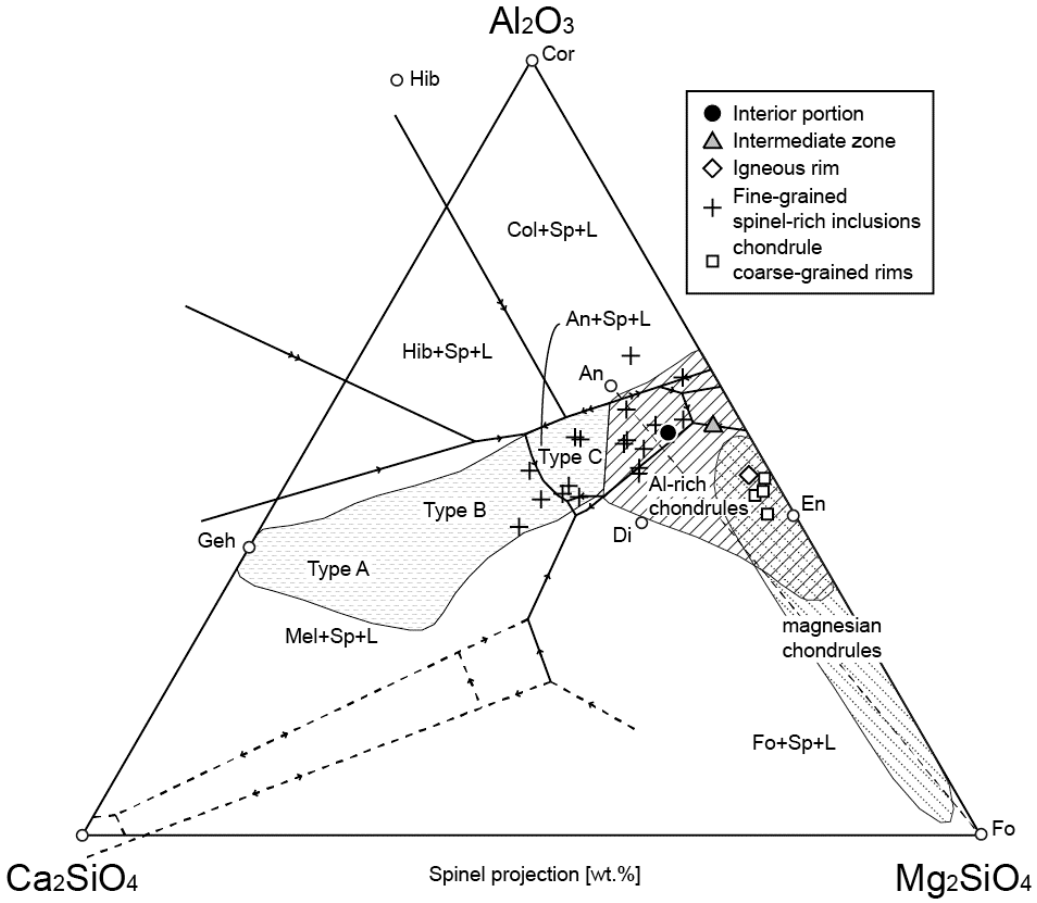
Al2O3
Cor
Hib
Interior portion
Intermediate zone
Igneous rim
Fine-grained spinel-rich inclusions
chondrule
coarse-grained rims
Col+Sp+L
An+Sp+L
Hib+Sp+L
An
Type C
Al-rich chondrules
En
Type B
Geh
Di
Type A
Mel+Sp+L
magnesian chondrules
Fo+Sp+L
Fo
Ca2SiO4
Spinel projection [wt.%]
Mg2SiO4

Fig. 7 a) The bulk rare earth element (REE) abundance pattern of the WI-025 interior portion. The typical abundance pattern of group II CAI is plotted as a reference. All REE abundances are normalized to CI chondrite abundances (Anders and Grevesse, 1989). b) Mixing model between hypothetical CAI and chondrules (see text). The crosses and broken lines are the calculated REE abundance patterns of CAI-chondrule mixtures with a CAI component of 20, 40 and 80 wt. % as shown. Calculated REE abundance pattern of a CAI-chondrule mixture with a 40 wt. % CAI component resembles the WI-025 interior portion in its LREE abundances, small La/Lu ratio and small negative Eu anomaly.

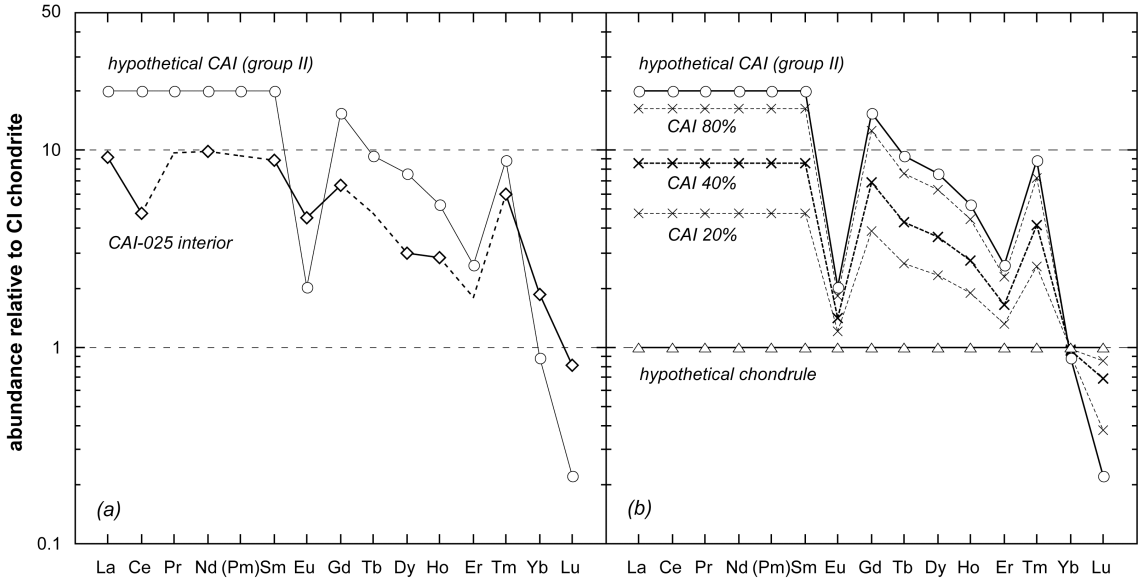

Fig. 8 Oxygen isotopic compositions of minerals in WI-025. The white, black and gray symbols represent the analyses of the interior portion, the igneous rim and the intermediate zone, respectively. The oxygen isotopic composition in WI-025 is heterogeneous among minerals. The oxygen isotopic compositions of the olivines and low-Ca pyroxenes from all three areas are all distributed in a narrow range despite the very different textures observed in these three areas. TFL and CCAM correspond to terrestrial fractionation line and carbonaceous chondrite anhydrous mineral line, respectively.

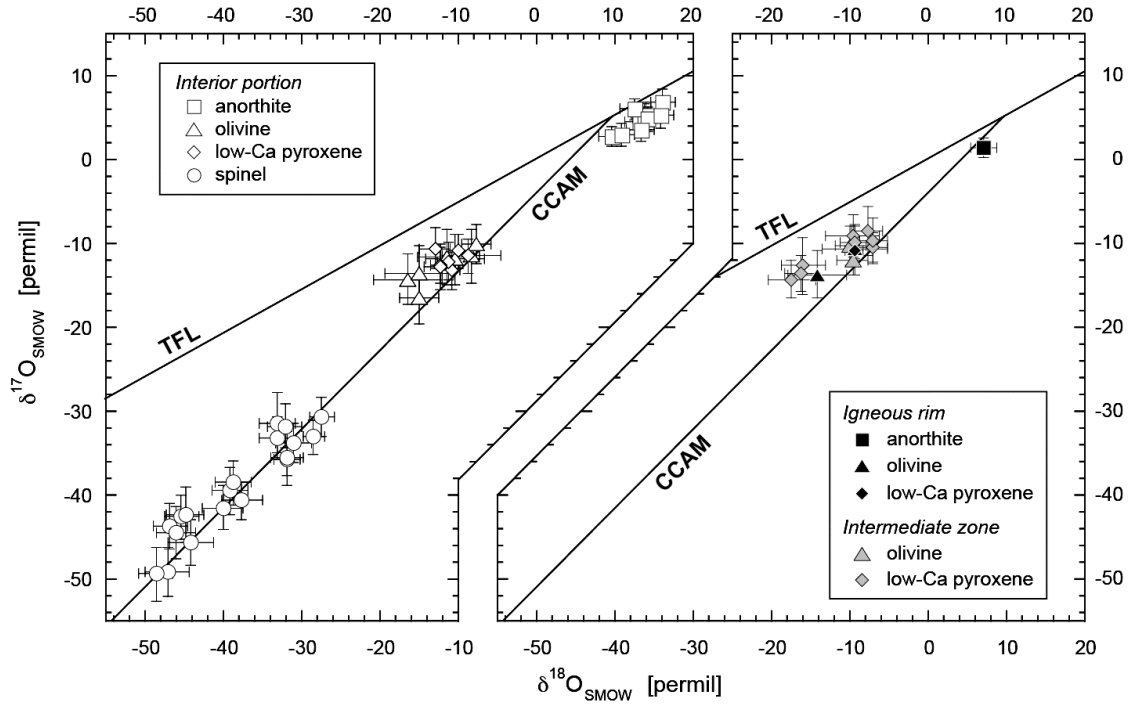

Fig. 9 The oxygen isotopic compositions of olivines and low-Ca in the interior portion, the igneous rim and the intermediate zone are compared by $\Delta^{17}O$ value. The horizontal lines and gray areas are the weighted average and 2 sigma errors for each mineral and area, respectively. The ^{16}O-enrichment of olivines and low-Ca pyroxenes in all three areas is essentially identical within analytical error.

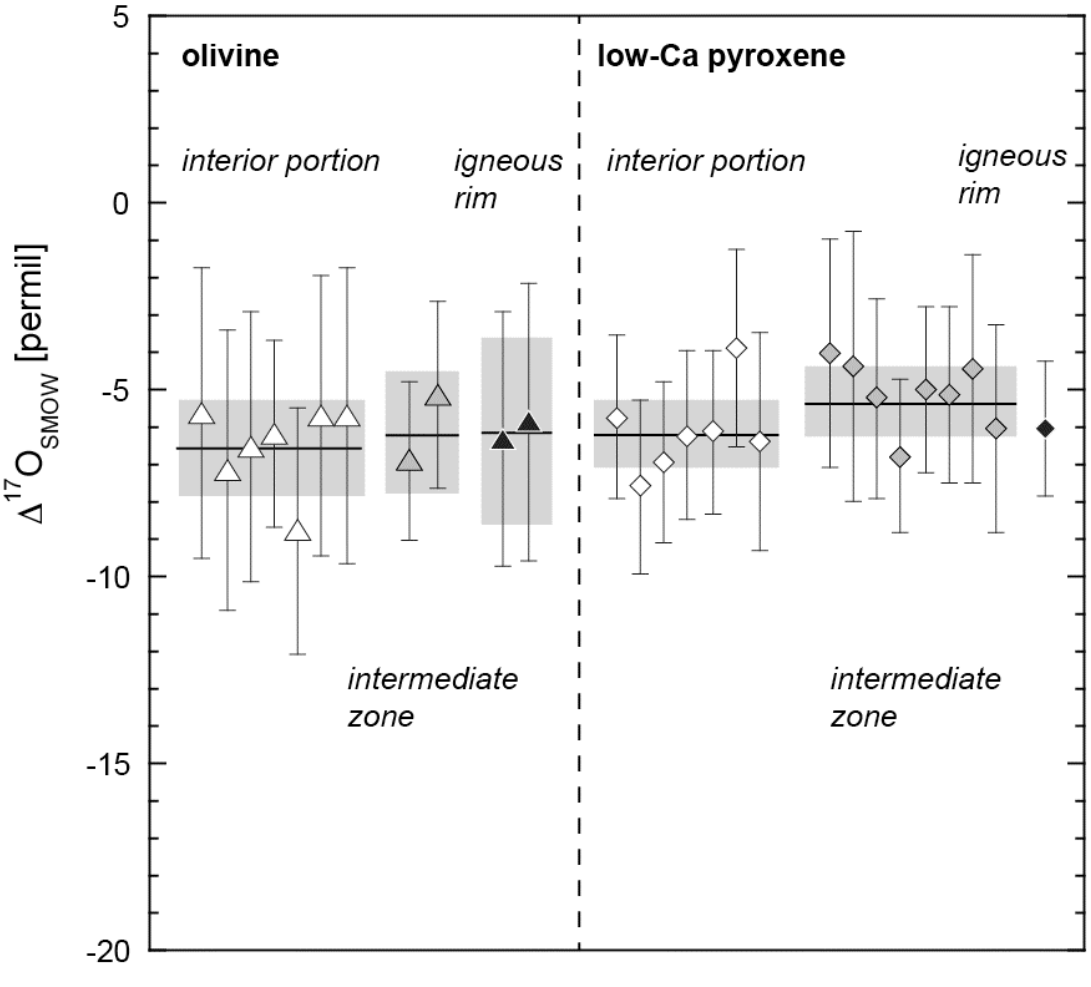

Table 1 Trace element compositions of WI-025 interior portion.

	Sc	Cr	Co	Zn	La	Ce	Nd	Sm	Eu	Gd	Dy	Ho	Tm	Yb	Lu	Re	Os	Ir	Au
nuclide	^{46}Sc	^{51}Cr	^{60}Co	^{65}Zn	^{140}La	^{141}Ce	^{147}Nd	^{153}Sm	^{152}Eu	^{153}Gd	^{166}Dv	^{166}Ho	^{170}Tm	^{175}Yb	^{177}Lu	^{186}Re	^{191}Os	^{192}Ir	^{198}Au
energy (eV)	889.3	320.1	1333	1116	1596.5	145.4	91.1	103.2	121.8	97.4	82.5	80.6	84.3	396.3	113	137.1	129.4	468.1	411.8
half-life	84.0 d	27.8 d	5.26 y	245 d	40.3 h	32.5 d	11.0 d	46.7 h	13.3 y	241 d	81.5 h	26.8 h	129 d	4.19 d	6.71 d	90 h	14.6 d	74.4 d	2.70 d
abundance [ppm]	8.80	3208	457	11	2.17	2.87	4.47	1.31	0.25	1.30	0.73	0.16	0.14	0.30	0.020	< 0.04*1	< 0.2*1	0.14	0.028
error(1σ)	0.09	32	5	2	0.05	0.27	0.65	0.01	0.01	0.14	0.14	0.06	0.07	0.02	0.004	-	-	0.01	0.005
abundance / CI chondrite*2	1.51	1.21	0.91	0.04	9.3	4.8	9.9	8.9	4.5	6.6	3.0	2.8	6.0	1.9	0.8	< 1	< 0.4	0.29	0.2

*1 Detection limit was estimated from 3SD of the background counts for each spectrum.

*2 CI chondrite abundances of these elements used for nomalization were taken from Anders and Grevesse (1988).

Table 2 Representative major element compositions of minerals in WI-025.

mineral	anorthite		spinel			olivine						Low-Ca pyroxene						
location	interior portion	interior portion	interior portion	interior portion	interior portion[*1]	interior portion	interior portion	intermediate zone	intermediate zone	igneous rim	igneous rim	interior portion	interior portion	interior portion	intermediate zone	intermediate zone	igneous rim	igneous rim
Oxide [wt.%]																		
Na2O	1.5	0.5																
MgO	0.1		26.9	27.9	24.1	56.1	55.0	51.9	53.5	51.2	49.4	32.4	34.3	36.2	35.3	37.4	37.0	37.7
Al2O3	32.9	34.9	69.8	69.6	68.7							12.6	9.8	2.9	5.4	2.9	1.8	1.1
SiO2	46.1	43.8		0.3		42.1	42.4	41.2	41.9	41.3	40.9	49.8	52.7	57.1	55.2	57.4	57.3	58.1
CaO	17.4	19.1										0.4	0.4	1.3	0.9	0.3	0.5	0.4
TiO2				0.3								2.6	1.3	0.6	0.5	0.2	0.4	
Cr2O3			0.8	1.4	2.0							0.6	1.0	0.7	1.0	0.8	0.5	0.4
FeO			1.8	0.9	7.1	0.7	3.5	5.9	3.9	7.1	9.4	0.4	0.5	0.5	0.6	0.6	0.6	0.7
Total	98.0	98.3	99.3	100.4	101.9	98.9	100.9	99.0	99.3	99.6	99.8	98.8	100.0	99.3	98.9	99.6	98.1	98.4
Cation No,																		
Na	0.13	0.04																
Mg	0.01		0.97	0.99	0.87	1.98	1.93	1.88	1.91	1.85	1.80	1.65	1.73	1.83	1.79	1.88	1.89	1.92
Al	1.82	1.94	1.98	1.95	1.95							0.51	0.39	0.12	0.22	0.11	0.07	0.04
Si	2.16	2.06		0.01		1.00	1.00	1.00	1.00	1.00	1.00	1.70	1.78	1.94	1.88	1.94	1.96	1.98
Ca	0.87	0.96										0.01	0.01	0.05	0.03	0.01	0.02	0.02
Ti				0.00								0.07	0.03	0.02	0.01	0.01	0.01	
Cr			0.02	0.03	0.04							0.02	0.03	0.02	0.03	0.02	0.01	0.01
Fe			0.04	0.02	0.14	0.01	0.07	0.12	0.08	0.14	0.19	0.01	0.01	0.01	0.02	0.02	0.02	0.02
Total cations	5.00	5.00	3.00	3.00	3.00	3.00	3.00	3.00	3.00	3.00	3.00	3.97	3.98	3.98	3.98	3.99	3.99	3.99

[*1] Fe rich spinel which is in contact with the intermediate zone.

Table 3 Bulk major element compositions of WI-025 normalized to 100%.

area	No. of analysis	Na_2O (wt.%)	MgO	Al_2O_3	SiO_2	S	Cl	K_2O	CaO	TiO_2	Cr_2O_3	FeO	NiO
interior portion	37	0.7	17.7	36.0	33.9	<0.1	0.1	<0.1	9.8	0.2	0.6	1.0	0.1
intermediate zone	16	8.0	16.7	20.6	40.1	0.5	1.8	0.1	4.3	0.3	0.5	6.9	0.3
igneous rim	18	3.1	20.7	13.3	34.3	2.1	0.3	0.2	2.4	0.2	0.8	20.1	1.5

Table 4 Oxygen isotopic data of minerals in WI-025.

Analysis number	$\delta^{17}O$ (‰)	2σ	$\delta^{18}O$ (‰)	2σ	$\Delta^{17}O$ (‰)	2σ
anorthite (interior portion)						
an 01	4.5	1.5	13.1	1.8	-2.3	1.8
an 02	5.2	1.7	14.0	1.8	-2.0	1.9
an 03	5.0	1.7	13.8	1.6	-2.2	1.9
an 04	6.9	1.5	16.1	1.6	-1.4	1.7
an 05	6.0	1.3	12.6	1.9	-0.6	1.7
an 06	4.8	1.5	14.2	1.6	-2.5	1.7
an 07	5.4	1.6	15.8	1.8	-2.8	1.9
an 08	3.5	1.4	13.3	1.7	-3.4	1.6
an 09	2.7	1.2	9.7	1.7	-2.3	1.5
an 10	3.0	1.4	10.8	1.7	-2.6	1.7
weighted mean (2SE)					-2.2	0.5
anorthite (igneous rim)						
an 11	1.3	1.2	7.0	1.7	-2.3	1.5
spinel (interior portion)						
sp 01	-33.1	2.1	-28.4	1.4	-18.3	2.2
sp 02	-35.7	2.1	-31.8	1.7	-19.1	2.2
sp 03	-30.6	2.4	-27.4	1.5	-16.4	2.5
sp 04	-45.7	2.7	-44.2	2.9	-22.7	3.1
sp 05	-43.7	2.8	-46.8	2.1	-19.4	3.0
sp 06	-49.2	2.9	-47.2	2.8	-24.7	3.3
sp 07	-33.8	2.4	-31.0	2.3	-17.7	2.6
sp 08	-33.1	2.5	-33.2	2.1	-15.9	2.7
sp 09	-41.5	2.7	-40.1	2.5	-20.7	3.0
sp 10 [*1]	-40.7	2.3	-37.7	2.6	-21.1	2.7
sp 11	-42.6	2.6	-45.3	2.2	-19.0	2.9
sp 12	-35.6	3.2	-31.8	2.1	-19.0	3.4
sp 13	-49.4	3.2	-48.6	2.2	-24.2	3.4
sp 14	-39.5	2.8	-39.1	2.3	-19.1	3.1
sp 15	-42.3	3.3	-44.8	2.4	-19.0	3.5
sp 16	-44.5	3.0	-46.0	2.4	-20.5	3.3
sp 17	-31.4	3.6	-33.1	2.3	-14.2	3.8
sp 18	-38.5	2.6	-38.8	2.3	-18.4	2.8
sp 19	-31.8	2.6	-32.1	2.2	-15.1	2.9

Table 4 Continued.

Analysis number	$\delta^{17}O$ (‰)	2σ	$\delta^{18}O$ (‰)	2σ	$\Delta^{17}O$ (‰)	2σ
low-Ca pyroxene (interior portion)						
px 01	-10.9	2.1	-10.0	1.3	-5.7	2.2
px 02	-13.2	2.2	-10.9	1.2	-7.6	2.3
px 03	-11.5	2.0	-8.8	1.4	-6.9	2.1
px 04	-12.1	2.2	-11.3	1.4	-6.2	2.3
px 05	-12.5	2.1	-12.3	1.1	-6.1	2.2
px 08	-10.6	2.4	-12.9	2.0	-3.9	2.6
px 09	-12.8	2.7	-12.4	2.1	-6.4	2.9
weighted mean (2SE)					-6.2	0.9
low-Ca pyroxene (intermediate zone)						
px 07	-9.1	2.5	-9.7	3.4	-4.0	3.1
px 10	-12.7	3.3	-16.0	2.8	-4.4	3.6
px 11	-14.3	2.2	-17.4	3.0	-5.2	2.7
px 12	-10.5	1.8	-7.1	1.9	-6.8	2.1
px 13	-9.9	2.0	-9.4	2.0	-5.0	2.2
px 14	-13.6	2.1	-16.3	2.2	-5.1	2.4
px 15	-8.5	2.9	-7.8	2.0	-4.4	3.0
px 16	-9.7	2.6	-7.0	1.7	-6.1	2.8
weighted mean (2SE)					-5.3	0.9
low-Ca pyroxene (igneous rim)						
px 06	-10.9	1.7	-9.4	1.1	-6.0	1.8
olivine (interior portion)						
ol 01	-11.6	3.3	-11.4	3.8	-5.6	3.9
ol 02 (lath)	-11.5	3.2	-8.3	3.8	-7.1	3.7
ol 03	-11.9	3.0	-10.4	3.8	-6.5	3.6
ol 05 (lath)	-10.1	2.3	-7.7	1.8	-6.2	2.5
ol 08	-16.6	3.0	-15.0	2.5	-8.8	3.3
ol 09	-14.3	3.0	-16.5	4.4	-5.7	3.7
ol 10	-13.5	3.3	-15.0	4.3	-5.7	4.0
weighted mean (2SE)					-6.6	1.3
olivine (intermediate zone)						
ol 06	-11.9	1.9	-9.6	2.0	-6.9	2.1
ol 07	-10.3	2.3	-9.9	2.0	-5.1	2.5
weighted mean (2SE)					-6.2	1.6
olivine (igneous rim)						
ol 04	-13.7	2.8	-14.2	3.7	-6.3	3.4
ol 11	-10.7	3.0	-9.3	4.1	-5.9	3.7
weighted mean (2SE)					-6.1	2.5

[*1] Analysis of Fe rich spinel in contacvt with the intermediate zone.